5-2021

A Geoarchaeological Site Formation Model at Alm Shelter, Wyoming

Cayla Kennedy
Utah State University

A GEOARCHAEOLOGICAL SITE FORMATION MODEL

AT ALM SHELTER, WYOMING

by

Cayla Kennedy
A thesis submitted in partial fulfillment
of the requirements for the degree

of

MASTER OF SCIENCE

in

Anthropology

Approved:

_____	_____
Judson Byrd Finley, PhD. Major Professor	Erick Robinson, PhD. Committee Member
_____	_____
Tammy Rittenour, PhD. Committee Member	Jacob Freeman, PhD. Committee Member

_____

D. Richard Cutler, PhD.
Interim Vice Provost for Graduate Studies

UTAH STATE UNIVERSITY
Logan, Utah

2021

ABSTRACT

A Geoarchaeological Site Formation Model

at Alm Shelter, Wyoming

by

Cayla Kennedy, Master of Science

Utah State University, 2021

Major Professor: Dr. Judson Byrd Finley

Department: Sociology, Social Work, and Anthropology

Understanding the environmental context of archaeological sites plays an important part in interpretation of human behavior and informs the scale and timing of regional climatic shifts. Alm Shelter is a rockshelter located on the western margin of the Bighorn Mountains in Wyoming and contains one of the most complete late Pleistocene and Holocene rockshelter stratigraphic sequences in context with archaeological data. Geoarchaeological investigations at this site address the timing and nature of significant environmental events, as well as comparing these to other regional studies. This study presents new stratigraphic analysis, sedimentology, luminescence ages, and an OxCal age-depth model as a proxy for local and regional environmental change. The new environmental data are compared to other regional climate studies to test whether periods of eolian sedimentation at Alm Shelter reflect larger patterns across the western United States. Results indicate a refined chronology using radiocarbon ages and additional grain-size analysis is necessary, but loose connections to major trends in regional

aridity during the late Pleistocene and early Holocene can be made across the Bighorn Basin, Wyoming, the eastern Great Basin, and northern Great Plains. These connections can be used to inform human decisions and behavior during periods of drastic environmental change.

(95 pages)

PUBLIC ABSTRACT

A Geoarchaeological Site Formation Model

at Alm Shelter, Wyoming

Cayla Kennedy

Alm Shelter, located in north-central Wyoming, is an archaeological site with a long history of human occupation. This study addresses new contextual information in the form of dated sediment deposits, analysis of sediment types, and a computer model to assist with identifying climate conditions that may have led to periods of significant change. Using the model, it is possible to estimate the timing of environmental shift as well as other events that may not be directly dateable. This information is then compared to other sites containing climate records to determine if conditions at Alm Shelter are connected with other locations in a larger pattern. The results indicate that this model is not ideal for precise connections with other sites but does demonstrate two clusters of possible dry conditions that are loosely connected with other locations, including other archaeological sites in the Bighorn Basin and geological and climate studies at sites in Wyoming, the eastern Great Basin, and the northern Great Plains. This information is important for understanding patterns of human movement and decision-making when conditions become very dry.

ACKNOWLEDGMENTS

Thanks are due to many individuals and organizations for their generous support of this study. To my advisor, Dr. Judson Finley, thank you for asking me to work on this project, for many rounds of meetings, edits, playing in the dirt, and for providing the means to work through my degree program. I am grateful to Dr. Tammy Rittenour, Dr. Erick Robinson, and Dr. Jacob Freeman for agreeing to sit on my committee, and for their invaluable assistance in the development of this manuscript. I thank Dr. Robert Kelly for his generous assistance with funding the laboratory work, as well as his patience in answering many emails asking for information. This research was funded in part by a National Science Foundation Senior Archaeology research award (Award #1939019) to Dr. Kelly. Additionally, I would like to thank the Society for American Archaeology and the Geological Society of America: Geoarchaeological Division for their generous financial contributions to the cost of this research. I would like to thank the staff of the USU Luminescence Laboratory – Michelle Nelson, Maggie Erlick, and Carlie Ideker – or their assistance in processing and testing the samples.

My experience through graduate school would not have been the same without the camaraderie of Paige Dorsey, Kelly Jimenez, Alix Piven, and Gideon Maughan, as well as various members of other USU Anthropology cohorts. Thank you to Darcy Bird for assistance with RStudio programming. Finally, thank you to my mom, my family, and my friends. Many tragedies and complications happened during my graduate education, and I am grateful for their unending support throughout. This manuscript honors the late Dr. George Frison, without whom Wyoming archaeology would not be what it is today. It is also in honor of my brother, Cody Kennedy, though he would likely have rolled his eyes if he saw this.

LAND ACKNOWLEDGMENT STATEMENT

The data collection and excavations at Alm Shelter were conducted on an ancestral Indigenous archaeological site that occupies lands of the Absaalooke (Crow) Nation, and the bands of the Eastern Shoshone Tribe. The Utah State University Logan campus, where I studied and conducted the majority of this research, occupies the traditional homeland of the Northwestern Band of Shoshone Indians. I acknowledge these Indigenous communities and their ancestors as the stewards of the land and keepers of knowledge from time immemorial.

CONTENTS

Page

LIST OF TABLES

Page

LIST OF FIGURES

Page

Regional climate reconstructions in the western United States often face issues reconciling variable climate in topographically diverse environments (Nicholson et al. 2019). Comparison of individual sites against other multi-proxy reconstructions is necessary in order to determine local versus regional signals of climate change. When examining human-environment interactions, this distinction between local and regional signals is essential to understanding environmental pressure on human populations, as local-only signals may not reflect larger patterns in paleodemographics (Wright 2011). Stratified deposits at archaeological sites provide an important bridge between human activity and biogeomorphic conditions. Rockshelters provide protection from the elements and thus provide an excellent source for stratified deposits (Woodward and Goldberg 2001).

The Bighorn Basin presents an excellent study area because it is a topographically diverse landscape and exhibits strong regional biogeomorphic reactions when precipitation shifts (Lyford et al. 2002). Hundreds of rockshelters are in the western margin of the Bighorn Mountain Range. Many contain evidence of human activity, and few contain long sequences of undisturbed stratified deposits (Finley 2008; Kornfeld et al. 2010). This study presents a geoarchaeological analysis of site formation processes at Alm Shelter, Wyoming as a proxy for Holocene paleoenvironmental conditions to compare against regional climate studies.

Alm Shelter, located along Paintrock Creek near Hyattville, Wyoming (Figure 1), is a limestone rockshelter with a nearly complete late Pleistocene through Holocene sedimentary sequence (Finley 2008). Because it is one of the more complete regional sequences, Alm Shelter can serve as a key point of comparison with similar sites. It also provides an important independent test for local and regional paleoenvironmental reconstructions (Kelly et al. 2013; Nicholson et al. 2019; Shuman et al. 2010). Eolian deposits can indicate periods of aridity,

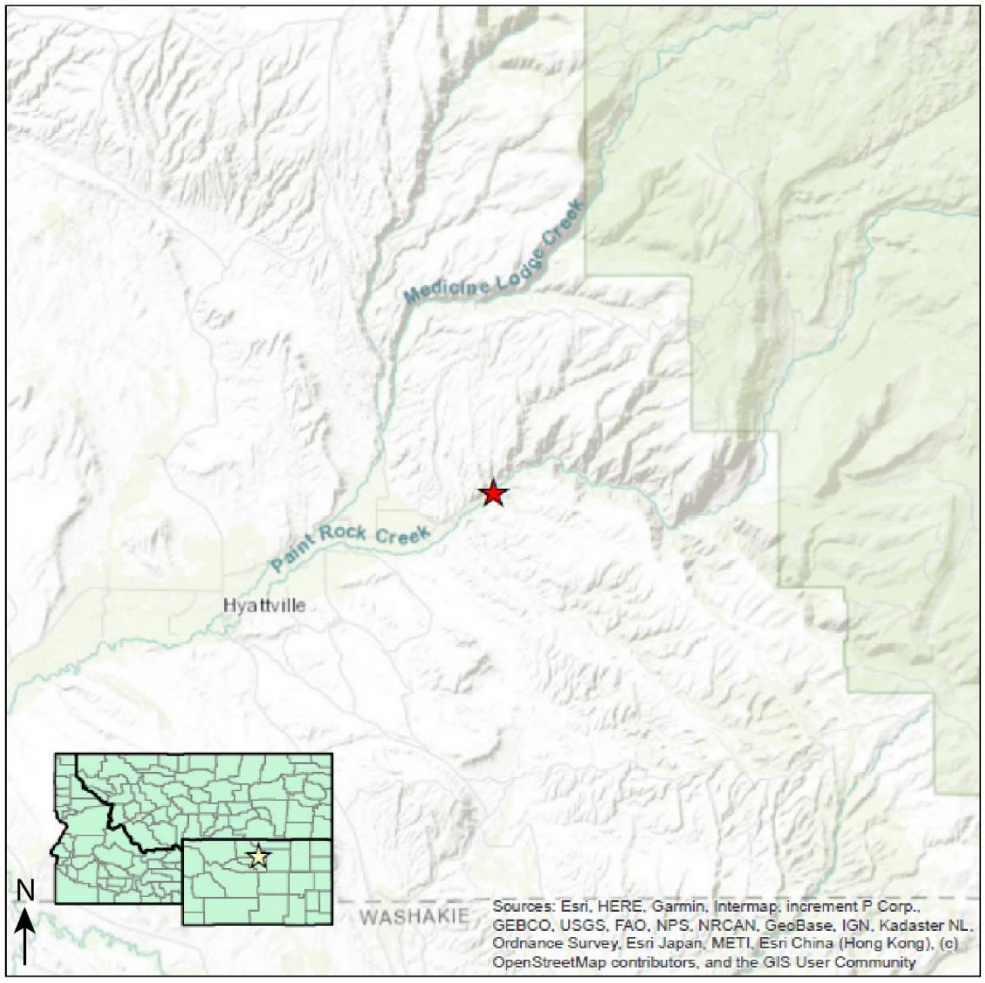

Figure 1. Location of Alm Shelter site.

and rockshelters like Alm Shelter present conditions conducive to trapping sediment and protecting them from erosional forces (Busacca et al. 2003; Surovell et al. 2009). This paper addresses three primary objectives: first, establishing the site geoarchaeological context through field and laboratory descriptions using stratigraphic profiles, grain-size analysis, and luminescence analysis; second, creation of a Bayesian age-depth model for age constraints on eolian units and key stratigraphic transitions; and third, comparison of the Alm Shelter record to regional eolian records to evaluate the extent and timing of drought signals in patterns of

Holocene environmental variability. Following Finley (2008, 2016), this study tests the hypothesis that the Bighorn Basin rockshelter record preserves centennial-scale aridity events via eolian sedimentation, and that these events correspond to regional patterns of increased aridity. It begins with a review of the Bighorn Basin rockshelter record and provides contextual information used in the interpretation of the stratigraphic record of Alm Shelter. Next, this paper describes the methods used in the reconstruction of the biophysical context of the Alm Shelter deposit and age-depth model, followed by the results of the stratigraphic, sedimentological, and geochronological analysis. Finally, it examines the age-depth model as a method for constraining the age of eolian deposition and the results of comparison to other eolian records as a test for local signals of regional environmental change.

The results signal a general agreement with both the luminescence ages and the stratigraphic relationships of the model, as well as some correlation between the local model and several regional climate reconstructions. At Alm Shelter, a transition from alluvial to colluvial sedimentation occurred in the late Pleistocene, followed by fluctuating periods of eolian deposition through the early Holocene. In addition to the construction of a site depositional history and a contextual chronological model for human occupation at Alm Shelter, this information also aids future studies in understanding the consequences of regional drought on population dynamics as well as the regional movement patterns of humans during periods of drastic climatic shifts. This will inform future implications of drought on demographics in the rapidly approaching climate crisis (Warner et al. 2010).

Project Setting

The Bighorn Basin and adjacent Bighorn Mountains are part of the Central Rocky Mountain physiographic province located in northwestern Wyoming (Fenneman 1931). The basin is bounded by the Pryor Mountains to the north, the Absaroka Range and Yellowstone Plateau to the west, the Bighorn Mountains to the east, and the Owl Creek Range to the south. Elevations in the region range from 1100 m (3600 ft) at the lowest point of the Bighorn Basin to greater than 4000 m (13,100 ft) at Cloud Peak in the Bighorn Mountains. Major drainages include the Bighorn River, as well its two principal tributaries, the Greybull and Shoshone Rivers. Many smaller tributaries occur in the Bighorn and Absaroka ranges and converge in the basin.

Due to the high mountain ranges on the boundaries of the Bighorn Basin, it and the western slope of the Bighorn Mountains lie within a double rain shadow, emphasizing the effects of fluctuating effective moisture (Martner 1986; Mitchell 1976). Pacific moisture travels inland in the winter, though much of the precipitation occurs in the Yellowstone Plateau west of the basin. Gulf of Mexico moisture travels northwest in the summer but dissolves over the eastern side of the Bighorn Mountains. Winter temperatures in the basin range from -16.5 to 0.5 degrees Celsius (2.2 to 33.0 degrees F), whereas summer temperatures range from 33.1 to 13.3 degrees Celsius (91.6 to 56.0 degrees F), (WRCC 2021). On the western slope of the Bighorn Mountains, winter temperatures range from -14.4 to 0.2 degrees Celsius (32.4 to 6.1 degrees F), and summer temperatures range from 32.1 to 12.4 degrees Celsius (54.3 to 89.7 degrees F). Average annual

precipitation is 6.48 inches in the basin, while the western margin averages 25.5 cm (WRCC 2021).

Vegetation consists of drought-tolerant species similar to that of the Great Basin, including currant, Utah juniper, greasewood, mountain big sagebrush, Great Basin wildrye, rabbitbrush, prickly pear cactus, yucca, and mountain mahogany (Knight 1994). Due to this unique placement between high-elevation mountains, the Bighorn Basin contains primarily sparse desert vegetation with pockets of riparian environments near perennial streams, particularly in the canyons of the western slope of the Bighorn Mountains (Knight 2014). Because of this, declines in effective moisture are likely to have a marked effect on vegetation change and thus erosion and sediment transportation.

During the Eocene Epoch approximately 50 million years ago, the Laramide orogeny uplifted and formed the Central Rocky Mountains via continental crustal compression (Brown 1993). Major Paleozoic sedimentary formations exposed in the Bighorn Mountains during major downcutting of Bighorn River tributaries include Madison (Mississippian) limestone, Amsden (Mississippian-Pennsylvanian) limestone and sandstone, and Tensleep (Pennsylvanian-Permian) sandstone (Boyd 1993). The Bighorn Basin sedimentary formations include Mesozoic Chugwater and Morrison sandstone formations, as well as other siltstones and shales along the basin-foothills margin (Picard 1993; Steidtmann 1993). Central Bighorn Basin deposits are primarily Eocene Willwood Formation fine-grained sedimentary deposits (Pierce 1997). Alluvial transportation of fine-grained sediment like the Willwood Formation are a vital source of material for eolian deposits, particularly right as arid conditions begin to increase (Knox 1972).

The sedimentary structures in the western slope create rockshelters in three geomorphic settings: Madison paleokarst, Pleistocene active karst, and fluvial erosion of sandstone (Finley

2008). The Madison paleokarst pockets were excavated via the retreat of the Mississippian Sea and filled with limestone roof fall, sand, silt, and shale during the Pennsylvanian period (Sando 1974; Sando 1978). Rockshelters in the paleokarst are frequently located on high-angle slopes and cliffs, and fill sediments erode out easily due to poor cementation (Finley 2008). Active karst formed in the early Pleistocene (around 600 ka) and followed the path of water downslope from the upper reaches of the Bighorn Mountains (Sutherland 1976). Tensleep sandstone rockshelters form primarily through autogenic granular disintegration. Tensleep sandstone itself is particularly susceptible to weathering due to mature, rounded quartz grains cemented by anhydrite or dolomite (Boyd 1993). Sedimentation in Bighorn Basin rockshelters can be separated into two primary methods: allogenic and autogenic (Woodward and Goldberg 2001). Allogenic sedimentation refers to external sources of sedimentation, including eolian, fluvial, and colluvial transportation. Allogenic sedimentation frequently occurs with well-rounded and smooth sediment grains due to increased friction while the grain is in motion (Tate et al. 2007) Autogenic sedimentation denotes grains from inside the rockshelter itself, separated from the bedrock through weathering processes.

Archaeology of the Central Rocky Mountains

The archaeological record of the Northwest Plains and Middle Rocky Mountains is generally divided into three broad categories: Paleoindian, Archaic, and late Prehistoric (Kornfeld et al. 2010). Paleoindian archaeology is generally defined as a series of cultural

complexes dominated by large game hunting with limited evidence of plant processing, although it is reasonable to assume that plants and small game were an important part of Paleoindian diets (Byers and Ugan 2005). Individual Paleoindian cultural complexes are primarily identified through stone tool technologies like the fluted and stemmed lanceolate projectile point (Kornfeld et al. 2010). The timeline for the Paleoindian period is continually being updated by older sites but is currently understood to be 16,000-10,000 cal yr BP in western North America (Davis et al. 2019). Archaic technology, though heavily variable by region, is defined by the trend toward the incorporation of smaller game and plants in diets, as well as smaller notched and stemmed projectile points. The Archaic period in the Northwest Plains and Central Rocky Mountains lasted from approximately 8,500-1,500 cal yr BP and is divided into three phases (i.e., Early Archaic ca. 8,000-5,500 cal yr BP, Middle Archaic 5,500-3,500 cal y BP, and Late Archaic 3,500-1,500 cal yr BP) each with distinct diagnostic projectile point styles and regional settlement strategies (Kornfeld et al. 2010). The Late Prehistoric transition is generally marked by the appearance of bow-and-arrow technology, and later, earthenware pottery (Finley et al. 2017; Kornfeld et al. 2010). The addition of the Protohistoric period in the western United States is also variable depending on the time European-Americans made contact regionally in the last decades of the 18th century and the first decades of the 19th century.

Bighorn Basin Archaeology

While early Paleoindian occupations are known in the Bighorn Basin (Finley et al. 2005; Frison and Bradley 1980; Frison and Todd 1986; Todd et al. 1987; Kornfeld et al. 2010), the Paleoindian record is dominated by the Foothill-Mountain Paleoindian complex, an early shift

towards broad spectrum foraging and reduced mobility (Frison 2007). Archaic technology in the Bighorn Basin is well-preserved, particularly in rockshelters due to their relative protection from erosion and weathering. Rockshelters and caves may have served as refuge from harsh weather conditions, including periodic droughts (Albanese and Frison 1995; Anderson 2007). Plains and Western Macrotradition stone tools, stone-filled fire pits, evidence of residential structures, food remains, wood, and fiber objects comprise some of the recovered Archaic artifacts in the Bighorn Basin (Frison 2007; Frison and Walker 2007; Husted 1995; Kornfeld 2007). Late Prehistoric and Protohistoric components are also evident in many of the archaeologically significant rockshelters, including stone tools and ceramics attributed to the ancestral Crow (Frison and Walker 2007).

Archaeological investigations in the Bighorn Basin, particularly in regional rockshelters, began in 1938 and continues through today (Kornfeld 2007; Husted 1964; Frison 1962; Frison 1968; Frison 1973; Frison 2007; Frison and Walker 2007; Finley 2008). Dinwoody Cave, excavated in 1938 and 1939 by the Works Project Administration (WPA), produced over 600 artifacts, though these were returned to the Wind River Reservation and reinterred due to the site's spiritual significance (Kornfeld 2007; Francis and Loendorf 2002). Birdshead Cave (Bliss 1950), excavated in 1947 under a salvage archaeological project for Boysen Reservoir, contained seven occupation levels, demonstrating an early understanding of long-term continued occupation in the Bighorn Basin and surrounding region. Other archaeological investigations occurred during 1960s salvage work in Bighorn Canyon, uncovering artifacts at several rockshelters, including Sorenson, Bottleneck, and Mangus Caves, and confirmed the mid-Holocene presence of humans in this region (Husted 1964). These sites produced many Middle and Late Archaic perishables, as well as other materials through the late Prehistoric and post-

European contact periods. Rockshelter research in the Bighorn Basin is most well-known from Frison's legacy of research, beginning in the early 1960s and including sites like Daugherty Cave, Spring Creek Cave, Leigh Cave, and Medicine Lodge Creek, (Frison 1965; Frison 1968; Frison and Huseas 1968; Frison and Walker 2007). Many of these sites exhibit Paleoindian occupation, indicating a late Pleistocene to early Holocene use of the Bighorn Basin and Bighorn Mountains. Medicine Lodge Creek remains among the most important regional sites because it contains the most refined chronology of occupation due to over five meters of relatively intact alluvial stratigraphy (Frison and Walker 2007). These sites were essential in refining not only the Bighorn Basin cultural chronology, but the prehistoric occupation sequence for the Central Rocky Mountains and Northwest Plains (Kornfeld et al. 2010).

Surovell et al. (2009) use over 800 published and unpublished radiocarbon ages from around the Bighorn Basin in order to create and test a model of taphonomic bias, defined as increased presence of younger sites due to cumulative, destructive effects of erosion on older sites. They postulate that open-air sites in the Bighorn Basin are disproportionally affected by taphonomic bias because they are unlikely to be buried and preserved, whereas closed sites act like sediment traps and lead to burial and preservation of archeological data. Using their model to correct for taphonomic bias, Surovell et al. (2009) demonstrate that open-air site and rockshelter use was nearly identical except for the periods between 9,500-7,000 cal yr BP and 4,000-2,000 cal yr BP, where rockshelter use exceeds open-air sites and indicates that the foothills locations where rockshelters occur were more intensively occupied during drought cycles.

Bighorn Basin rockshelters provide important geological tests of human response to environmental change because the stratigraphic deposits are local records of biogeomorphic

response to climate change (Finley 2008, 2016). Alm Shelter is one of the best examples as it contains a nearly complete stratigraphic record spanning the late Pleistocene and Holocene. With proper analysis and chronological control, the Alm Shelter stratigraphic record can be exported to other rockshelters as a key to understanding the chronology of geomorphic events and cultural occupations that is a complimentary record to Medicine Lodge Creek (Frison 2007; Ostahowski and Kelly 2014). Previous archaeological work includes test excavations in the early 2000s by the University of Wyoming, as well as several recent seasons of excavations in the main unit. Excavation revealed nearly two meters of deposits with significant amounts of cultural materials (Craib et al. 2019). During more than 10 years of excavations, radiocarbon and luminescence samples have produced a robust archaeological and geoarchaeological chronology. This paper presents initial findings from luminescence samples, grain-size analysis, and stratigraphic analysis to create a local model of rockshelter site formation for comparison against other regional proxies of environmental change. These records collectively reveal the timing and spatial extent of Holocene droughts spanning the eastern Great Basin, Central Rockies, and into the western High Plains.

Holocene Eolian Record and Environmental Change in the Interior Western US

Understanding shifting effective moisture conditions in the past is key to understanding potential patterns in the present and future. Information such as changing species of pollen, amounts of certain minerals, and evidence of deposition regime changes assist researchers in

identifying paleoclimate patterns and can assist in developing new models for understanding the future. Periods of eolian sedimentation generally reflect increased aridity (Busacca et al. 2003; Dean et al. 1996; Clarke and Rendell 1998). In eolian sedimentation, sediment supply is highest at the beginning of droughts, as alluvial processes deposit sand when the carrying capacity of the flowing water decreases (Knox 1972). Eolian sedimentation is primarily driven by sediment availability and supply, transport capacity of water, vegetation cover, and moisture conditions, as well as consistent wind to entrain and move fine-grained sediment (Ahlbrandt et al. 1983; Busacca et al. 2003; Kocurek and Lancaster 1999). While eolian activity is often connected to greater aridity, some studies suggest that more frequent precipitation events may lead to increased fluvial deposition of well-sorted sediments, adding to sediment supply in overbank depositional environments (Bullard and Livingstone 2002; Clarke and Rendell 1998). Eolian activity declines during periods of increased effective moisture when vegetation cover increases anchoring of otherwise mobile sediments. During drier conditions, an inverse relationship between decreased vegetation cover and increased sediment mobility is present (Hugenholtz and Wolfe 2005; Knox 1972). Using a local model from information found at Alm Shelter, this information regarding aridity can be exported and tested to determine whether arid conditions persisted around the western interior of the continent.

Paleoclimate Records of the Western United States

Continuous and discontinuous paleoenvironmental data, taken from lake and wet meadow cores as well as dune records across the western United States, provide vital context for

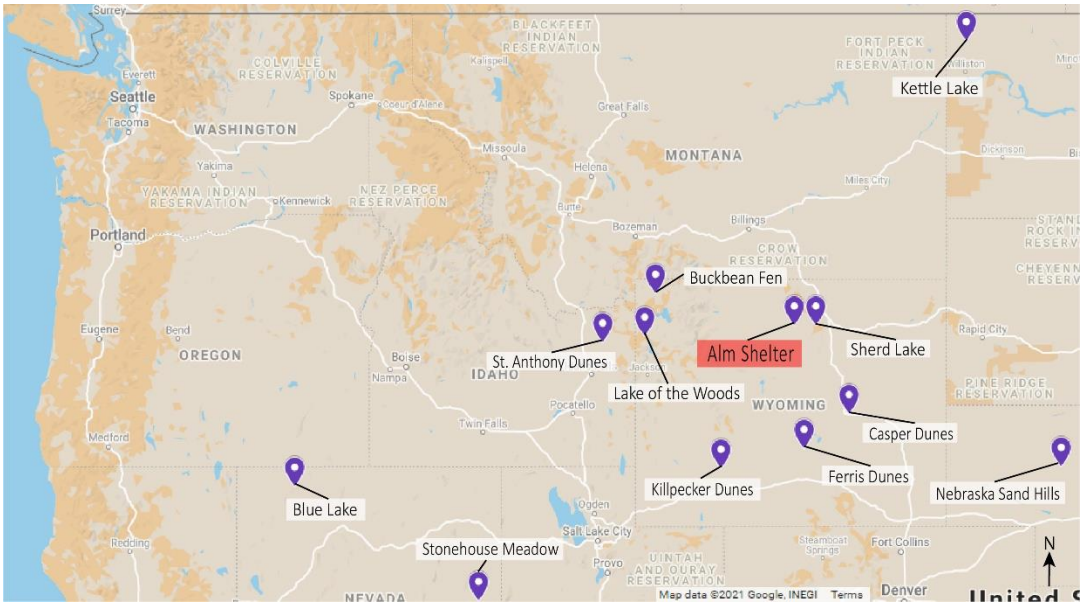

Figure 2. Regional paleoclimate study sites.

the Alm Shelter record (Figure 2). These selected studies reflect major periods of decreased effective moisture, with goals of determining regional and continental patterns of aridity. All ages in this study are presented in calibrated years before present (cal yr BP) beginning at AD 1950, including the luminescence ages presented from Alm Shelter (Wolff 2007). Some comparative studies cited here initially presented ages in uncalibrated radiocarbon years before 1950 (14C yr BP) while others present ages in kiloannum (ka) measures. Results originally presented in ^{14}C yr BP were calibrated using the CALIB software (Stuiver et al. 2021), and results presented in ka were corrected by subtracting the difference between year of publication and 1950 to match outputs from the age-depth model (Bronk Ramsey 2008; Bronk Ramsey and Lee 2013). The following comparative studies here contain various error margins, as older samples are compared against newer samples subject to advancements in technology that led to increased precision in both radiocarbon and luminescence dating methods.

The interior western US has many well-known eolian landscapes that provide strong evidence for shifting Holocene environmental conditions, as these landscapes require consistent or intense periods of aridity to demonstrate activation in their sedimentation record (Knight et al. 2004). Sand dune records, while temporally discontinuous, hold a vital place in understanding timing of drought cycles with enough intensity to initiate dune activation. The following studies use luminescence to bracket spans of dune activation and contextual radiocarbon ages to bracket spans of soil formation (Ahlbrandt et al. 1983; Forman et al. 2005; Halfen et al. 2010; Loope et al. 1995; Mayer and Mahan 2004; Miao et al. 2007; Stokes and Gaylord 1993; Stokes and Swinehart 1997). Lake records discussed here are another important and continuous contribution to understanding climate records in the western United States (National Research Council 2006). Lake records can include sediment cores that contain pollen, mollusks, diatoms, and minerals that track fluctuations in effective moisture and temperature (Grimm et al. 2011; Louderback and Rhode 2009; Mensing et al. 2013; Shuman et al. 2010; Shuman 2012; Shuman and Marsicek 2016).

Dune Records. Dune fields in the basins of the Central Rocky Mountains and interior western United States provide important evidence for the timing and regional extent of Holocene environmental change and provide increased regional context for sites in Wyoming like Alm Shelter (Alhbrandt et al. 1983; Halfen et al. 2010; Mayer and Mahan 2004; Stokes and Gaylord 1993). These records are defined as discontinuous because they track discrete events like dune stabilization and activation, rather than a continuously resolved deposit like varved lake cores. Important Wyoming localities include the Killpecker Dunes, Ferris Dunes, and Casper Dunes (Figure 2). Geochronological methods provide complementary views of eolian conditions where radiocarbon dating of soils are evidence for dune stabilization and soil formation requiring more

mesic conditions, while luminescence dating reconstructs dune mobilization and decreased effective moisture (Alhbrandt et al. 1983; Halfen et al. 2010; Mayer and Mahan 2004; Stokes and Gaylord 1993). The Killpecker Dunes and the Casper Dunes have been studied by geologists to understand timing of activation and stabilization, and this is reflected in the use of both radiocarbon and luminescence dating methods (Ahlbrandt et al. 1983; Halfen et al. 2010; Mayer and Mahan 2004). The Ferris Dunes and its associated stratigraphic record have been primarily documented using radiocarbon dating methods (Stokes and Gaylord 1993).

Documentation of aridity from the St. Anthony Dunes in eastern Idaho are included to provide context west of the study site, and the luminescence ages track dune activations around the core of the dune field (Rich et al. 2015). However, western United States dune records outside of Wyoming primarily come from the western Great Plains, including the Nebraska Sand Hills (Figure 2). These records are important to compare against Alm Shelter to confirm periods of widespread arid conditions (Ahlbrandt et al. 1983; Forman et al. 2005; Loope et al. 1995; Miao et al. 2007; Stokes and Swinehart 1997). These records are again established with both luminescence and ^{14}C ages, sampled from eolian dune activity and interdunal soil formation respectively.

Moisture and Temperature Records. Bighorn Basin climate reconstructions, using pollen and lake level records from Lake of the Woods, Buckbean Fen, and Sherd Lake, found that prolonged periods of aridity and higher temperatures occurred throughout the Holocene (Shuman et al. 2010; Shuman 2012). The Lake of the Woods record tracks changes in effective moisture using sediment cores and ground penetrating radar measurement of shoreline elevations changes over time, based on the assumption that silt and mud accumulate continuously in deep water while sand accumulates in shallow water (Shuman et al. 2010). Shuman (2012) presents

reconstructed data from Buckbean Fen and Sherd Lake using comparisons between fossil pollen and favored temperature conditions of seven groups of modern pollen analogs. These three site records are discontinuous and may represent local patterns.

Three climate proxies from the western United States provide important continuous temperature and moisture records outside of the Central Rocky Mountains that may be affected by widespread environmental trends (Figure 2). Estimated periods of aridity in Blue Lake, Nevada were tracked using an age-depth model of ^{14}C ages from plant macrofossils, peat, and organic carbon from bulk mud samples, as well as accumulation rates of different pollen types in the sediment cores (Louderback and Rhode 2009). Like Blue Lake, Stonehouse Meadow, Nevada, uses sediment cores to demonstrate periods of increased Holocene aridity but also includes sediment analysis, identification of terrestrial pollen and mollusks with specific moisture requirements, identification of diatom flora, and ^{14}C ages taken from bulk charcoal-rich sediment, mollusks, and seeds (Mensing et al. 2013). The Kettle Lake, North Dakota varve records are based on sediment cores, ^{14}C ages taken from plant macrofossils, pollen identification, and comparison of calcite and aragonite dominance in sections of the cores demonstrating differences in groundwater flow (Grimm et al. 2011).

At Alm Shelter, periods of aridity were determined using grain-size analysis and luminescence dating. The grain-size analysis is key to determining whether sandy strata represent wind-blown sediment and luminescence dating to providing age control of these depositional packages (Tate et al. 2007).

Methods

Geoarchaeology

Research at Alm Shelter began in 2005 with excavation of a single 1-x-1-m test unit, designated as the TP 1 test unit (Figure 3). Two additional test units were excavated in 2009, which were designated TP 2 and TP 3. Both units were excavated closer to the shelter interior (Figure 3). Excavations were expanded between 2014 and 2018 to create a block connecting the TP 1, 2, and 3 test units. The main stratigraphic profiles come from the south wall of TP 1, the south wall of the TP 2 test, and the west wall of the main block. Profiles were drawn using reference to the master excavation grid at the site with elevations recorded in depths below the site datum using an arbitrary elevation of 100.00 m. Field profiles mapped a representative sample of boulders larger than 10 cm as critical reference points for future investigations. Boulder concentrations are also useful markers of stratigraphic contacts in rockshelter deposits. Sediment descriptions follow USDA Soil Survey nomenclature (Soil Survey Staff 1999).

Bulk sediment samples were collected for grain-size analysis. Sediment samples from the west wall of the excavation block were analyzed in the USU Geoarchaeology Lab and the USU Geochemistry Lab. Sediment samples were split and weighed to create a base sample weight. Using two nested screens and a solid pan, the samples were manually sieved to separate cobbles and pebbles (> 2 mm), granules (1-2 mm), and coarse to fine sand (<1 mm). Each size classification was weighed to determine percentage of cobbles, pebbles and sand based on the

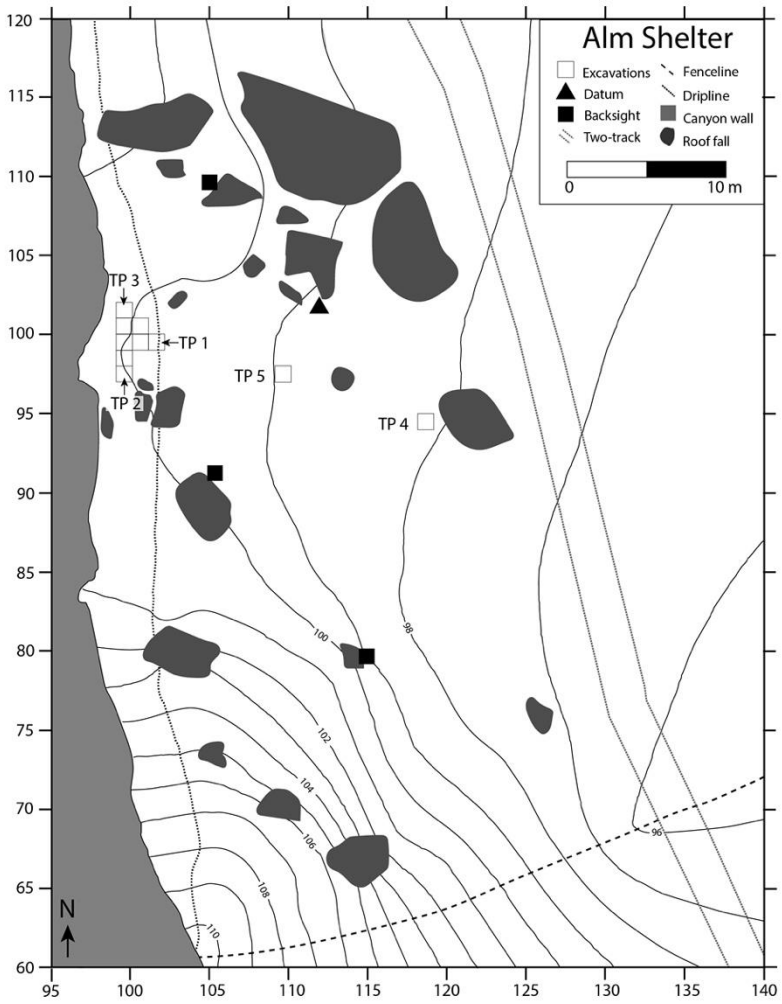

Figure 3. Planview map of Alm Shelter indicating main excavation unit and test pits. Modified from Ostahowski and Kelly (2014).

Wentworth (1922) classification scheme. Grain-size distributions were measured using a Malvern Mastersizer 2000 with Hydro 2000 MU attachment. This equipment uses laser diffraction in order to determine size distribution down to 0.02 microns. Laser diffraction uses predictable patterns of scattered light from the laser striking various particle sizes to translate into grain-size measurements (Malvern Instruments 2007). Sediment analysis used the following protocol. The pump was set to 3,000 revolutions per minute, and a program of three

measurements for 30 seconds was selected in order to establish accurate and precise measurements for each sample. Once the computer program and instrument were prepared, a small, representative amount of sediment was added into the beaker of DI water until the laser obscuration level on the Malvern reached 7-10%. One minute of sonication assisted in breaking apart clumps of material before the material analysis took place. Results from the Malvern as well as the manual sieve of the samples were entered into a spreadsheet in order to determine percentages of each grain-size classification.

Luminescence Dating

Many archaeological studies use luminescence dating to supplement or replace radiocarbon chronologies (Clarkson et al. 2017; Douka et al. 2014; Ferbrache 2019; Gliganic et al. 2012; Huckleberry and Rittenour 2014; Rittenour et al. 2015; Robbins et al. 2012). Luminescence provides ages on sediment deposition to inform paleoclimate reconstructions and site occupation chronologies. Eolian deposits are ideal for luminescence dating as the method requires fine-grained quartz and feldspar to produce ages (Stevens et al. 2006). When this fine-grained sediment is buried, trace radioactive elements in the surrounding matrix give off ionizing radiation, called the environmental dose rate (D_R), that collects in the electron traps of individual quartz and feldspar grains (Aitken 1998). The D_R is adjusted for the percentage of water present in the sample, as it attenuates the effect of radioactivity collecting in the electron traps (Guérin et al. 2011). The amount of absorbed radiation collected in these traps since burial from the sun is called the equivalent dose (D_E). When these sediments are stimulated by light or heat, the stored electrons are released from the trap in the form of photons. UV receptors capture the amount of

light released, and samples are then re-dosed with radioactivity and re-stimulated in increasing amounts to recreate the amount of radiation needed to produce the original light emission (Wintle and Murray 2006). Optically stimulated luminescence (OSL) measurements were performed on quartz grains stimulated with blue-green light (Huntley et al. 1985; Wintle and Murray 2006). Infra-red stimulated luminescence (IRSL) used infra-red stimulation on feldspar grains, with additional corrections for signal fading during the re-dose and re-stimulation phases (Auclair et al. 2003; Huntley and Lamothe 2001; Wallinga et al. 2000). D_R was calculated by measuring concentrations of radioactive elements such as potassium, uranium, thorium, and rubidium, as well as an estimate of contributed cosmic radiation. D_R is presented as Grays per thousand years, or Gy/kyr. Luminescence testing produces error margins of approximately 10% of the sample's age due to combined uncertainties of calculating D_R and D_E (Murray and Olley 2002).

Field collection of luminescence samples included both aluminum tube and film canister methods, under cloak of darkness, in order to accommodate thin lenses of targeted sediments. Three luminescence samples were collected from the base of the western wall (i.e., the west wall of the TP 3 test unit; Figure 3) in order to constrain the timing of the shift from the dominantly alluvial deposition of Paintrock Creek to colluvial and eolian sedimentation that characterizes most of the deposit. These three samples were collected by pounding 1.5 x 6" aluminum tubes into the base of the eastern wall. The tubes were packed with tissue and wrapped in light-proof tape at each end to prevent light contamination of the sediment inside. A quart-sized bag of sediment was collected from an approximately 30 cm diameter area around the sample to measure the dose rate. A film canister of sediment was collected for calculation of sediment moisture. Six additional luminescence samples were collected from the south wall of TP 2

(Figure 3), taken from distinct fine-grained deposits ideal for luminescence dating. These samples were collected under cloak of darkness by scraping a minimum of 5 mm of sediment from the selected deposits to prevent light contamination. A sediment sample was then collected into a light-proof film canister. Dose rate samples included a quart-size bag of sediment, and sediment water content samples were collected in film canisters.

Two additional luminescence samples, USU-3039 and USU-3040, were collected from TP 4 underneath a roof fall event outside the rockshelter dripline (Figure 3). The purpose of these samples was to determine the age of a major roof fall collapse of the shelter and further constrain the timing of the transition from the dominantly alluvial depositional regime to a subsequent regime of hillslope and eolian sedimentation. Both samples were collected under cloak of darkness, one with a film canister used for the luminescence, and the other with an aluminum tube. The film canister was used due to the presence of many larger cobbles directly underneath the boulder, while sediment lower in the stratigraphy allowed for a larger sample to be removed.

Lab Processing and Analysis. Eleven OSL samples were processed at the Utah State University Luminescence Lab in Logan, Utah under dim amber (590 nm) darkroom lighting to prevent potential bleaching of the luminescence signal. Each sample was wet sieved between 93-250 μm, with variations depending on the amount of initial material present. Isolation of the quartz and feldspar occurred by using 10% HCl and 3% H_2O_2 to remove carbonates and organic material. Two densities of sodium polytungstate were used in a double flotation process to isolate quartz (2.72 g/cm3) and feldspar (2.58 g/cm3) grains (Wallinga et al. 2000; Wintle and Murray 2000). The quartz samples underwent an additional process consisting of three 30-minute treatments of HF acid to remove any contaminating feldspars and etch the quartz, with a

final treatment of concentrated HCl to remove fluorite precipitates. D_R was calculated by inductively coupled plasma mass spectrometry (ICP-MS) and inductively coupled plasma atomic emission spectroscopy (ICP-AES) and using conversion factors of Guérin and colleagues (2011). In-situ water content was calculated by weighing the moisture samples, drying overnight in a 50º C oven, then weighing again to determine the percentage of water present in the sample.

Samples were tested for D_E using the single-aliquot regenerative-dose (SAR) method (Wallinga et al. 2000; Wintle and Murray 2006). OSL measurements of the fine quartz sand were conducted on a Risø TL/OSL DA-20 reader, using LEDs at 470±30 nm to stimulate 1-mm aliquots of quartz and a 7.5 mm UV filter for measurement of emitted light (Bøtter-Jensen et al. 2000). IRSL measurements were also made on the Risø TL/OSL DA-20 reader using 1-mm aliquots of feldspar grains and stimulated instead using 870 nm LEDs (Auclair et al. 2003). The IRSL samples were corrected for fading according to guidelines established by Huntley and Lamothe (2001). The Central Age Model (CAM) was used to calculate D_E of each sample (Galbraith and Roberts 2012).

OxCal Model

Modeling chronological and stratigraphic information in a Bayesian age-depth model is vital to interpolate ages of undated events in the sedimentary and archaeological records like stratigraphic boundaries and grain-size samples (Bronk Ramsey 2008). This interpolation is important for refining models of site formation and creating constraints for periods of major climatic shifts that cannot be directly dated. Age-depth models also help constrain comparisons with major regional shifts in this local record (Douka et al. 2014). OxCal incorporates Markov-

chain Monte Carlo (MCMC) simulations to aid in creating formal interpolation between ages in the stratigraphic sequence via the computation of a Bayesian probabilistic age-depth model, though this may come with additional imprecision (Bronk Ramsey 2008; Haslett and Parnell 2008; Parnell et al. 2011). In this study, the age-depth model was created using the Poisson sequence, or *P_sequence*, which allows for variation in the rate of accumulated sediments in the stratigraphic column. The stratigraphic information *z* and length of deposition *k* function as the *prior* information, while the ages inform the MCMC process in the *likelihood* (Bronk Ramsey 2008). The *posterior* information that results from the model are probability estimations about the selected ages; the start, end, and median ages of depositional sequences; and any additional non-dated material like grain-size samples or individual stratigraphic contacts, entered here as *Boundary* functions in order to produce a modeled age range.

Stratigraphic profile sketches drawn during excavation and sedimentological analyses informed insertion of the luminescence ages to reflect stratigraphic order into OxCal. *Prior* OSL ages were organized into depositional groups based on stratigraphic and grain-size evidence, inserted into the *P_sequence* using the *Date()* function, and run through the MCMC sequence. The k parameter was set to 100, using a variable *k* function rather than a fixed deposition rate to reflect variable sediment size and deposition rate throughout the several meters of sedimentary sequence (Bronk Ramsey and Lee 2013). The variability of *k*, inserted here as *D*, was set between 10^{-2} and 10^{2}, allowing the model to average the likely deposition rate between 1 and 10,000 depositional events per meter (Bronk Ramsey 2008; Bronk Ramsey and Lee 2013). The model uses an interpolation value of 0 because it incorporates modeling specific events using the *Boundary* function based on depositional history. The first iteration of the model uses *Boundary* to model ages of peak eolian events identified in the grain-size analysis, while the second

iteration models major depositional shifts identified in previous stratigraphic descriptions (Bronk Ramsey 2008; Finley 2008). Major climatic events identified in the regional climate models detailed above are compared to the *posterior* information from the age-depth model to determine whether Alm Shelter is reflecting local or regional climatic patterns.

Results

Stratigraphic Analysis

Stratigraphic analysis performed on TP 1 revealed a well-stratified deposit. Stratum 1 consists of compacted cow feces, while Strata 2 and 3 are fine-grained and stained with ash. Three primary depositional packages are identified between Strata 4 and 21: Strata 4-11 are fairly coarse with two fine-grained components, Strata 12-19 demonstrates an increase in fine-grain sediments with two gravel-dominated strata and two anthropogenic horizons, and Strata 20 and 21 both are massively bedded deposits, though Stratum 20 is gravel dominant while Stratum 21 is characterized by fine-grain sediments (Finley 2008). Stratigraphic descriptions are provided in Table 1 (Soil Survey Staff 1999). In order to maintain continuity of this analysis between the 2005 through 2018 excavations, both TP 2 and 3 as well as the western wall of the expanded excavation block follow the Finley (2008) stratum numbering (Figure 4). A one-meter block was skipped between the south walls of TP 1 and TP 2 (Figure 3). Strata from the south wall of TP 1 can be traced to the south wall of TP 2 (Figure 4), indicating lateral continuity east-west across the sedimentary deposits, with fine-grained deposits pinching out to the west and coarse grain

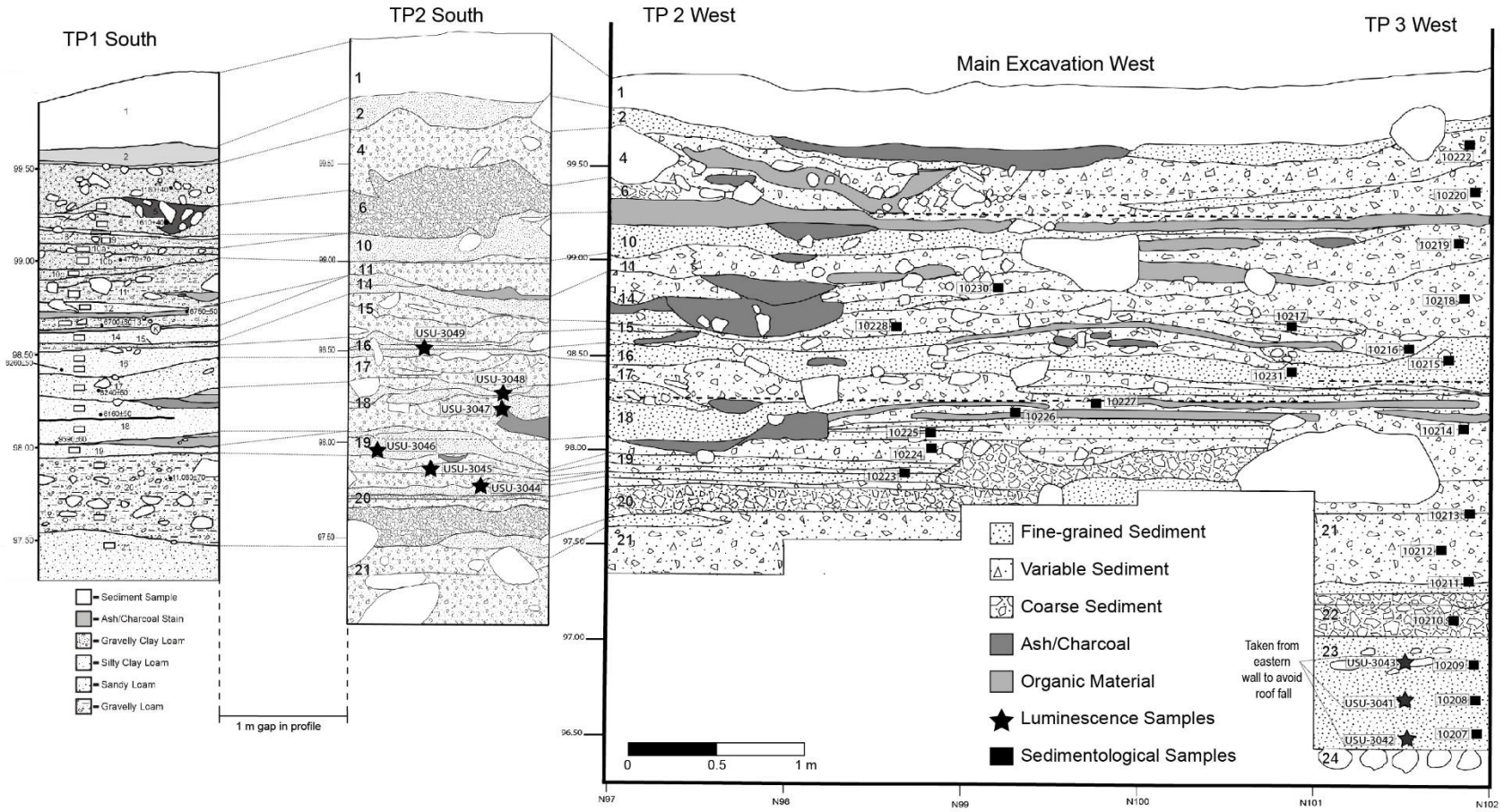

Figure 4. Stratigraphic profiles of TP 1, TP 3, TP 2, and the main excavation trench at Alm Shelter.

Table 1. Stratigraphic Descriptions from Alm Shelter TP 1 South Profile (Finley 2008).

Stratum	Description
1	Cow dung
2	Burnt limestone clasts and cow dung; 2.5Y8/1 (white)
3	Burnt cow dung; 2.5Y2.5/1 (black)
4	Gravelly silty clay loam; 10YR5/4 (yellowish brown); ~15% angular gravel; massive; loose (dry); slightly sticky, slightly plastic (wet); strongly effervescent; disseminated carbonates; clear, wavy boundary
5	Extremely gravelly sandy clay loam; 10YR4/3 (brown); ~15% angular to rounded gravel; single grain; loose (dry); sticky, slightly plastic (wet); violently effervescent; disseminated carbonates; abrupt, wavy boundary
6	Gravelly sandy clay loam; 10YR6/6 (brownish yellow); ~15% angular gravel; massive; soft (dry); sticky, plastic (wet); violently effervescent; disseminated carbonates; abrupt, smooth boundary
7	Sandy clay loam; 10YR6/4 (light yellowish brown); massive; soft (dry); sticky, plastic (wet); violently effervescent; disseminated carbonates; clear, wavy boundary
8	Silty clay loam; 10YR7/4 (very pale brown); massive; soft (dry); very sticky, plastic (wet); strongly effervescent; disseminated carbonates; abrupt, smooth boundary
9	Very gravelly sandy clay loam; 10YR5/4 (yellowish brown); ~30% angular gravel; single grain; loose (dry); slightly sticky, slightly plastic (wet); violently effervescent; disseminated carbonates; clear, smooth boundary
10a	Gravelly clay loam; 7.5YR3/2 (dark brown); ~20% angular gravel; massive; slightly hard (dry); slightly sticky, slightly plastic (wet); violently effervescent; disseminated carbonates; clear, smooth boundary
10b	Gravelly clay loam; 7.5YR4/4 (brown); ~20% angular gravel; massive; soft (dry); slightly sticky, nonplastic (wet); violently effervescent; disseminated carbonates; clear, smooth boundary
10c	Gravelly clay loam; 7.5YR4/6 (dark yellowish brown); ~20% angular gravel; single grain; soft (dry); slightly sticky, slightly plastic (wet); strongly effervescent; disseminated carbonates; clear, smooth boundary
11	Gravelly sandy loam; 10YR5/2 (grayish brown); ~20% angular gravel; single grain; loose (dry); nonsticky, nonplastic (wet); violently effervescent; disseminated carbonates; common, medium, oblong, white, noneffervescent salt; clear, wavy boundary
12	Clay loam; 10YR6/4 (light yellowish brown); massive, soft (dry); slightly sticky, slightly plastic (wet); violently effervescent; disseminated carbonates; common, medium, oblong, white, noneffervescent salt concentrated (many) on 1cm layer ~2cm above lower contact; clear, smooth boundary
13	Gravelly sandy loam; 10YR6/4 (light yellowish brown); ~20% angular gravel; massive; very friable (moist); slightly sticky, nonplastic (wet); strongly effervescent; disseminated carbonates; few, fine, oblong, white, noneffervescent salt; clear, smooth boundary

14	Clay loam; 10YR5/4 (yellowish brown); massive; very friable (moist); sticky, plastic (wet); violently effervescent; disseminated carbonates; clear, wavy boundary
15	Gravelly sandy loam; 10YR5/2 (grayish brown); ~20% angular gravel; massive; very friable (moist); slightly sticky, slightly plastic (wet); violently effervescent; disseminated carbonates; clear, smooth boundary
16	Sandy loam; 10YR6/6 (brownish yellow); massive, very friable (moist); slightly sticky, slightly plastic (wet); strongly effervescent; disseminated carbonates; clear, smooth boundary
17	Sandy loam; 10YR4/4 (dark yellowish brown); massive; very friable (moist); nonsticky, nonplastic (wet); violently effervescent; disseminated carbonates; common, fine to medium; oblong, white, non-effervescent salt; clear, wavy boundary
18	Silty clay loam; 7.5YR6/6 (reddish yellow); massive, friable (moist); slightly sticky, slightly plastic (wet); strongly effervescent; disseminated carbonates; few, fine, rounded, white, non-effervescent salt; clear, wavy boundary
19	Silty clay loam; 7.5YR5/6 (strong brown); massive, friable (moist); sticky, plastic (wet); violently effervescent; disseminated carbonates; clear, wavy boundary
20	Gravelly loam; 10YR5/4 (yellowish brown); >20% angular gravels and cobbles; massive; very friable (moist); slightly sticky, slightly plastic (wet); violently effervescent; disseminated carbonates; clear, wavy boundary
21	Loam; 10YR5/4 (yellowish brown); massive, very friable (moist); nonsticky, nonplastic (wet); violently effervescent; disseminated carbonates; no lower boundary

deposits pinching out to the east. Greater subdivisions of fine-grained sediments are more apparent on the south side of TP 2, particularly around Strata 16 and 18. Between Strata 19 and 20, there appears to be some additional subdivisions alternating between fine-grained and coarse-grained deposits. These thin lenses of fine-grained sediment were selected for luminescence testing.

The western wall of the main excavation block (Figure 4) demonstrates some continuity of the sedimentation patterns identified in TP 1 and TP 2. Toward the center of the excavation block and proceeding north toward TP 3, the distinction between stratigraphic layers becomes less clear, which may be related to the effects of cultural occupation. This section contains more

evidence of potentially cultural organic material mats and trampling of the somewhat finer-grained sediments may have blurred stratigraphic contacts. At the far north end, the western wall of the main excavation trench intersects TP 3. This unit was excavated an additional meter in depth revealing roof fall dominated deposits as a continuation of Stratum 21, a fine-grained deposit labeled here as Stratum 22, and a layer of well-rounded cobbles at the base of the excavation labeled as Stratum 23. This test was specifically designed to capture the pre-cultural geological depositional processes of the site, thus forming the basis for the site's formation history.

Grain-Size Analysis

Sedimentological samples were collected from the western wall of the main excavation trench, primarily from the western wall of TP 3 and the central portion of the main block (Figure 4). Samples from the western wall of TP 3 were taken from every stratum, while the samples from the western wall of the main excavation unit were taken from thin, fine-grained deposits suspected to be eolian events. From the 23 samples collected across the western wall, 15 contain greater than 50% fine-grain sediments. Four peaks of fine-grained sediments were identified throughout the stratigraphic column on the western wall (Figure 5). The strongest peak occurs at 1.32 meters below the datum (mbd) of excavation, with additional peaks at 1.55, 1.75, and 2.40 mbd. These peaks point to major changes in depositional regime, which correlate to the higher presence of fine-grained sediments in Strata 12-19. This two-prong approach appears to be a reliable indicator of increased transport of fine-grained sediment.

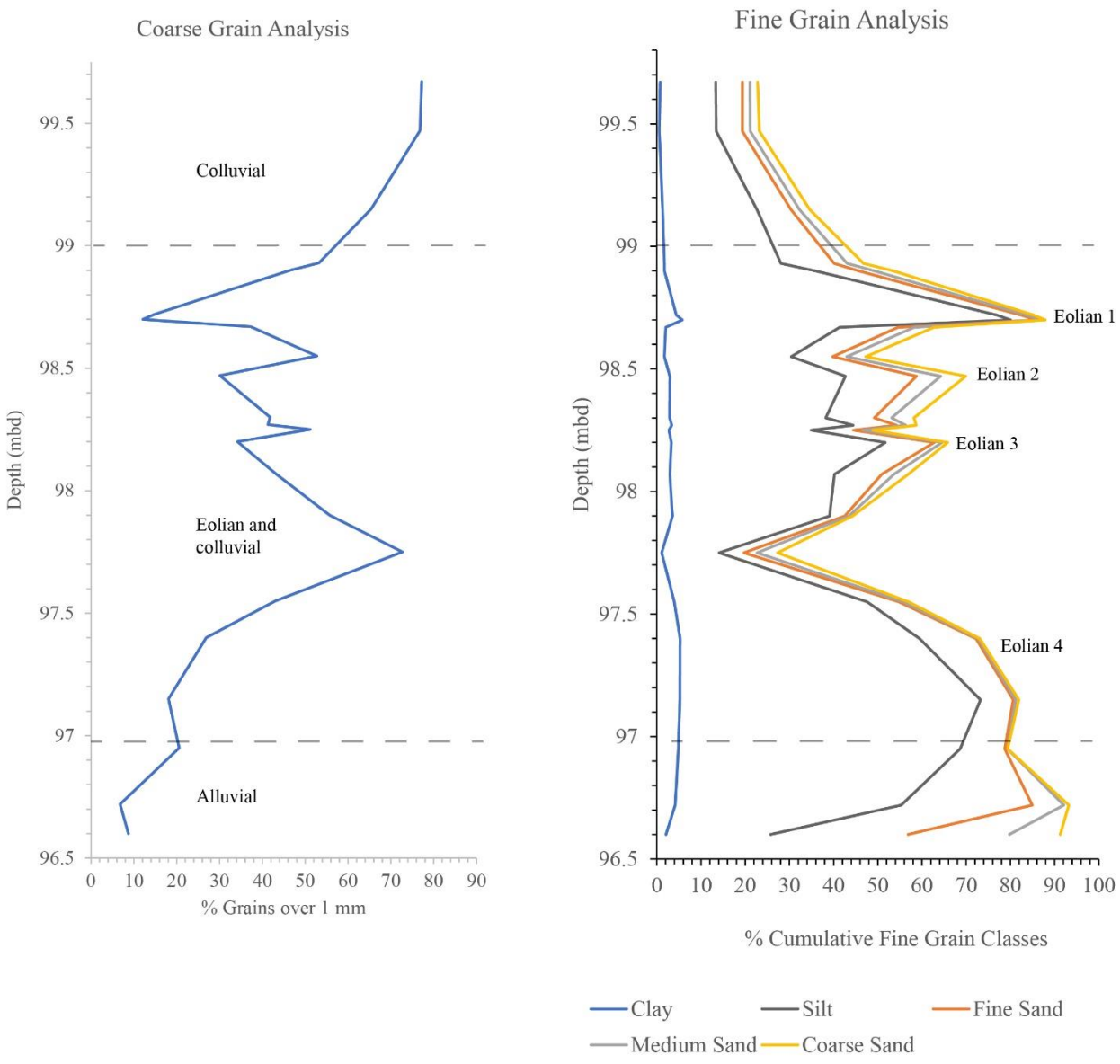

Figure 5. Grain-size analysis results with four peaks of eolian sedimentation highlighted.

OSL and IRSL

Results for the eleven luminescence samples are presented in Table 3. Luminescence samples were collected from three locations across the site. Two samples, USU-3039 and USU-

3040, were taken from an external test pit approximately 20 meters east of the main excavation block (Figure 3). Three samples were collected from the western wall of TP 3, while the remaining six samples were collected from the south wall of TP 2 (Figure 4). Two samples, USU-3044 and USU-3049, required IRSL analysis as there were few quartz grains remaining after the cleaning and mineral isolation process. Final ages were calculated using the Central Age Model, as no samples displayed signs of partial bleaching (Galbraith and Roberts 2012). Additionally, single-grain analysis was deemed unnecessary because the samples appeared to be well-bleached (Nelson et al. 2015). The ages are clustered in two main groups, with some overlap due to decreased precision: one in the terminal Pleistocene and the other in the early Holocene. The three samples from the eastern wall of TP 3 below Stratum 21 date to the late Pleistocene, between 18,250 ± 2,310 cal yr BP and 13,880 ± 1,880 cal yr BP, and were selected from culturally sterile deposits to constrain the pre-cultural formation of the site. Six samples from the south wall of TP 2, taken from fine-grained deposits between Strata 20 and 16, date to the terminal Pleistocene/early Holocene and range from 12,940 ± 1,400 to 7,160 ± 860 cal yr BP. The final two ages come from an external test unit underneath a roof fall event and date to 3,460 ± 730 directly underneath the boulder and 12,660 ± 1,870 cal yr BP about 80 cm below the boulder.

Table 2. Luminescence Age Information.

Location	USU num.	Depth (mbd)	Num. of aliquots[a]	Dose rate (Gy/kyr)	Equivalent Dose[b] ± 2σ (Gy)	Age ± 2σ (ka)	Method[c]	Age ± 2σ (cal yr BP)
TP 4	USU-3039	2.8	15 (32)	2.64 ± 0.10	33.66 ± 4.13	12.73 ± 1.87	OSL	**12,660 ± 4,130**
	USU-3040	2	16 (25)	2.26 ± 0.09	7.98 ± 1.51	3.53 ± 0.73	OSL	**3,460 ± 730**
TP 3	USU-3043	2.75	20 (30)	2.46 ± 0.10	34.37 ± 3.73	13.95 ± 1.88	OSL	**13,880 ± 1,880**
	USU-3041	3.2	18 (30)	2.44 ± 0.10	35.66 ± 4.29	14.59 ± 2.11	OSL	**14,520 ± 2,110**
	USU-3042	3.45	20 (22)	2.04 ± 0.08	37.35 ± 3.63	18.32 ± 2.31	OSL	**18,250 ± 2,310**
TP 2	USU-3049	1.37	18 (19)	3.23 ± 0.13	18.64 ± 1.63	7.23 ± 0.86	IRSL	**7,160 ± 860**
	USU-3048	1.57	15 (16)	1.79 ± 0.07	17.20 ± 1.16	9.63 ± 1.00	OSL	**9,560 ± 1,160**
	USU-3047	1.68	22 (26)	1.92 ± 0.07	17.75 ± 1.34	9.25 ± 1.01	OSL	**9,180 ± 1,010**
	USU-3046	1.82	15 (16)	1.91 ± 0.07	20.36 ± 1.22	10.69 ± 1.06	OSL	**10,620 ± 1,060**
	USU-3045	1.90	14 (16)	1.95 ± 0.07	20.32 ± 1.34	10.40 ± 1.07	OSL	**10,330 ± 1,070**
	USU-3044	1.98	17 (22)	2.89 ± 0.11	24.61 ± 1.77	13.01 ± 1.40	IRSL	**12,940 ± 1,400**

[a] Number of aliquots used in age calculation and total number of aliquots analyzed in parentheses.

[b] Equivalent dose (D_E) calculated using the Central Age Model (CAM) of Galbraith and Roberts (2012).

[c] Optically stimulated luminescence (OSL) age analysis using the single-aliquot regenerative-dose procedure of Murray and Wintle (2000) on 1-mm small-aliquots of quartz sand. Infrared stimulated luminescence (IRSL) age analysis using the single-aliquot regenerative-dose procedure of Wallinga et al. (2000) on 1-mm small-aliquots of feldspar sand at 50°C IRSL and corrected for fading following the method by Auclair et al. (2003) and correction model of Huntley and Lamothe (2001).

Age-Depth Model

General agreement between the stratigraphy and luminescence ages from Alm Shelter indicate no major age reversals that would present issues in the OxCal program. However, the large error terms of the luminescence samples result in a model that is relatively imprecise in terms of its ability to tightly constrain specific depositional events, as demonstrated by significant age overlap between samples. In order to refine the timing of depositional events, real and modeled luminescence ages were compared to other depositional indicators, and modeled ages were interpolated based on stratigraphic depth. Parameters for these models were set based on recommendations for age-depth models with multiple meters of deposition and flexible deposition rates, insertion of luminescence ages, and with the intent of using the *Boundary* function to model specific events (Bronk Ramsey 2008; Bronk Ramsey 2009; Bronk Ramsey and Lee 2013).

Sensitivity analyses were performed using various *k* and *p* parameters, but all convergence and agreement indices remained above acceptable limits of 95 and 60 respectively (Bronk Ramsey 2009). Figure 6a demonstrates the actual and modeled luminescence ages with the modeled ages from distinct fine-grained strata boundaries from the south wall of TP 1. Figure 6b uses the luminescence information with modeled ages from the four major eolian events identified in the grain-size analysis. Span and median ages for these modeled events are presented in Tables 3 and 4 and provide additional data to compare against regional climate studies. Generally, the modeled ages track specific time periods at which these eolian events took place, but error margins remain large due to the uncertainty of the luminescence ages used in the modeling process.

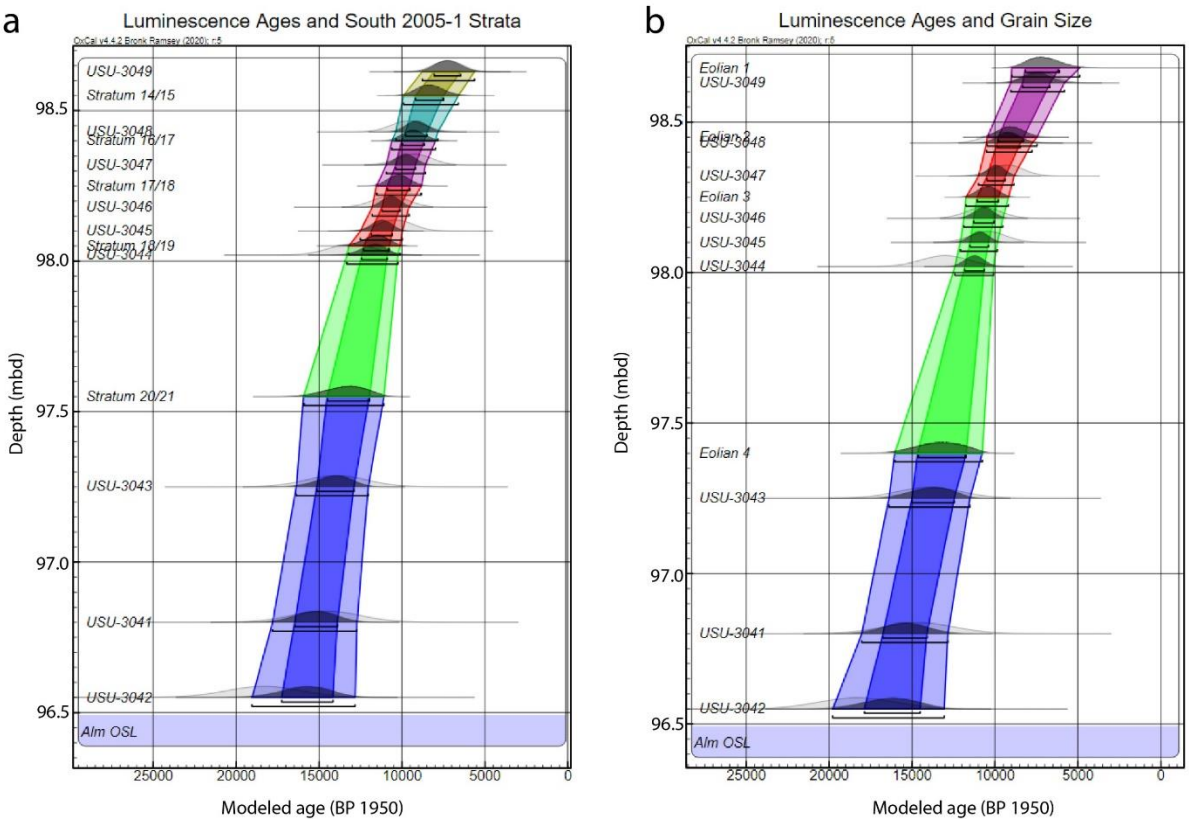

Figure 6. OxCal age-depth models from Alm Shelter.

Table 3. Modeled Ages of TP 1 Stratigraphic Contacts.

Depth (mbd)	Stratum Number	Median Modeled Age (cal yr BP)	Confidence Interval (95.4%)	Convergence Factor
1.45	14/15	8,310	1,600	99.2
1.6	16/17	9,320	1,300	99.2
1.75	17/18	10,160	1,350	99.1
1.87	18/19	11,580	1,640	98.8
2.45	20/21	13,320	2,620	98.3

Note: A_{model} 102.1, $A_{overall}$ 107.2

Table 4. Modeled Ages of Grain-Size Analysis Eolian Peaks.

Depth (mbd)	Name	Median Modeled Age (cal yr BP)	Confidence Interval (95.4%)	Convergence Factor
1.32	Eolian 1	7,080	1,900	99.2
1.55	Eolian 2	9,020	1,440	99.3
1.75	Eolian 3	10,440	1,310	99.4
2.6	Eolian 4	13,280	2,760	98.5

Note: A_{model} 108.9, $A_{overall}$ 114.7

Discussion

The purpose of this study is to examine the environmental context for the formation of Alm Shelter and compare it with other regional studies to determine the timing and scale of major periods of Holocene aridity across the interior western United States. Stratigraphic analysis, grain-size, luminescence ages, and an age-depth model confirm the presence and coarse-grained temporal distribution of eolian deposition at the study site that serves as a proxy for fluctuating moisture conditions. However, the comparison to the regional paleoclimate context is key in tracking regional events and determining whether Alm Shelter preserves isolated local events or major, widespread climatic phenomena. The results of this study present a comprehensive view of the site formation processes as revealed by the stratigraphy, sedimentology, and luminescence dating constrained within the OxCal age-depth model.

Site Formation History

The Alm Shelter sequence begins with deposition of a major package of Paintrock Creek alluvium following the Last Glacial Maximum (LGM) and at a time when the stream was at a higher base level and positioned against the cliff face. The basal deposits include a clast-supported matrix of well-rounded boulders associated with the bedload of Paintrock Creek (Strata 24: Figure 4). This latest Pleistocene depositional regime shifted to a phase of massively bedded sandy alluvium that is constrained by the lowest OSL age of 18,250 ± 2,310 cal yr BP (USU-3042; Figure 4), likely connected to the movement of Paintrock Creek from the western edge of the canyon toward the valley axis. Deposition of fine-grained alluvium continued for nearly 4,000 years, until 13,880 ± 1,880 cal yr BP (USU-3043: Figure 4) as indicated by the upper OSL age of Stratum 23. Strata 22 through 24 are only represented in the western section of TP 3 where the excavation continued an additional meter below the other units, although they likely occur across the site.

The second major phase of deposition at Alm Shelter began at 13,320 ± 2,620 cal yr BP (Strata 20/21: Table 3). This period is marked by the onset of roof fall accumulation and the development of debris fans from hillslope sediments above the rockshelter into the shelter interior on the north and south margins of the site (Figure 3). The debris fan on the southern edge of the site, best illustrated in the south walls of the TP 1 test and the TP 2 test, has considerable influence on the architecture and geometry of inset fine-grained sediment deposition. Where Stratum 20 in the south wall of the TP 1 test unit is one large continuous deposit, discrete lenses of fine-grained sediments are preserved closer to the debris fan in the TP 2 test that most likely pinch out in the meter between the two units. Additional subdivisions in the strata occur in the

south wall of TP 2 and continue approximately halfway through the western wall of the main excavation trench (Figure 4). Fine-grained sediment deposits during these periods were likely allogenic, though these appear to be preserved differently based on proximity to the debris fans (Finley 2008). These discrete lenses of fine-grained sediment most likely represent either pulses of eolian sedimentation, fluctuations in the intensity of coarse-grained sedimentation from the debris fan, or a combination of both processes. This is supported by the first of the fine-grained peaks identified in the grain-size analysis, between USU-3043 and USU-3044 (Figure 5; Table 3).

Luminescence ages of fine-grained sediments from Strata 20 through 16 in the south wall of the TP 2 test indicate regular eolian deposition between 12,940 ± 1,400 and 7,160 ± 860 cal yr BP (Table 3). Stratum 20 is marked by significant subdivision of sediment facies between TP 1 and TP 2, likely due to influence from the southern debris fan, and is constrained by luminescence ages between 12,940 ± 1,400 and 10,330 ± 1,070 cal yr BP. Like Stratum 20, Stratum 19 in the TP 2 test also has further facies subdivisions and is constrained by the luminescence age of 10,620 ± 1,060 cal yr BP and a modeled age from the upper stratigraphic boundary (Stratum 18/19 contact) of 11,580 ± 1,640 cal yr BP (Table 3). This reversal remains within error margins for the luminescence age but demonstrates the low precision of the age-depth model.

Stratum 18 appears to be subdivided with an additional coarse-grained deposit from the southern debris fan in the meter between TP 1 and TP 2. This stratum also contains two luminescence ages (USU-3047 and USU-3048), a modeled eolian peak (Eolian 3, Table 4), and a modeled stratum boundary (Stratum 17/18, Table 3), all between 10,500-9,100 cal yr BP. The lower margin of Stratum 16 marks the beginning of another pulse of fine-grained deposition,

with a modeled age of 9,320 ± 1,300 cal yr BP (Stratum 16/17: Table 3) and a luminescence age of 7,160 ± 860 cal yr BP as well as three subdivisions (Figure 4). Again, this reversal falls within the large error margins for the model. The modeled age from the Stratum 14/15 contact, a colluvial to eolian depositional regime change, occurs at 8,310 ± 1,600 cal yr BP (Table 3). The last modeled age for this phase is Eolian 1 peak at 7,080 ± 1,900 cal yr BP (Table 4).

The third depositional phase begins at Stratum 11 and is primarily marked by coarse-grained sediments, likely originating from the southern debris fan, interfingered with Strata 6 and 7, two very thin lenses of eolian sedimentation on the south wall of TP 1 (Finley 2008). These thin, fine-grained lenses pinch out toward TP 2 and the western wall of the main excavation unit (Figure 4). Strata 11 is constrained by three radiocarbon ages spanning 1,180 ± 40 to 4,770 ± 70 cal yr BP, dating this section of the deposit to the late Holocene. The upper strata in the western wall are largely flat, relatively level, and contain several layers of grass mats likely linked to anthropogenic activity. The increased cultural occupation from the early and middle Holocene at Alm Shelter likely caused some blurring of fine-grained deposit boundaries along the interior of the rockshelter behind the dripline. Strata 2 and 3 are charcoal-rich, fine-grained deposits with occasional small boulders from roof fall events. Stratum 1 is comprised of a large amount of compacted cow dung from historic settlement (Finley 2008).

Age constraints from the exterior test unit demonstrate the eastern downward slope as a result of the downcutting of Paintrock Creek. The presence of a 9,000-year gap in the luminescence ages on the hillslope well outside of the shelter apron indicates either an unconformity or an area of slower deposition, likely due to the test pit's position outside the dripline and subsequent reduced protection from erosional forces like the creek itself.

Paleoenvironmental Interpretation

The stratigraphy of Alm Shelter preserves a record of late Quaternary environmental change, including increased temperatures after the LGM. The earliest phase of site formation can be directly linked to deglaciation of the Bighorn Mountains. While direct evidence for the local timing of deglaciation is limited, Shuman and Serravezza (2017) report the earliest age of sediment deposition in Duncan Lake, a glacial lake at high elevation near Burgess Junction, as early as 17,000 cal yr BP. Licciardi and Pierce (2008) suggested retreat of alpine glaciers in the Beartooth Plateau on the western edge of the Bighorn Basin began by roughly 18,000 cal yr BP. Stable isotopes extracted from a stratified record of paleofecal materials at Last Canyon Cave at the base of the Pryor Mountains along the northern margin of the Bighorn Basin show increasing temperatures following the LGM with two temperature peaks at 14,400 cal yr BP and 13,5000 cal yr BP (Minckley et al. 2021), the latter of which appears to be reflected in the Alm Shelter record. Eolian sedimentation during the late Pleistocene is also recorded in the stratigraphy of Prospects Cave in the Little Mountain reach of the Bighorn Mountains between 18,000-10,000 cal yr BP (Finley 2008). Local temperatures decreased with the onset of the Younger Dryas around 12,800 cal yr BP (Minckley et al. 2021; Shuman and Serravezza 2017).

One response of alluvial geomorphic systems during the transition towards drier conditions is that sediment load is deposited faster due to decreased discharge and fine-grained sediment has a higher chance of wind-borne transportation (Knox 1972). This coupled process of decreased discharge and increased sediment availability is likely the source of fine-grained allogenic sediment in the Alm Shelter deposit. The stratigraphy of the Medicine Lodge Creek site, located a few km north of Alm Shelter and a tributary of Paintrock Creek, indicates a local

geomorphic context where sediment load vastly outpaced discharge, leading to deposition of massively bedded alluvial deposits dating to the late Pleistocene and early Holocene ca. 11,000-8,000 cal yr BP (Finley 2007). Medicine Lodge Creek alluvium is a probable source of fine-grained sediments transported into Alm Shelter through an eolian mechanism. This interpretation is somewhat at odds with Schuman and Serravezza's (2017) reconstruction of local lakes levels, which suggest increased moisture during the early Holocene between 11,000 — 8,000 years ago when regional lake levels rose. High sedimentation rates correspondent with increased regional moisture may reflect the availability of sediments following deglaciation and increased discharge resulting in greater overbank sedimentation in places like Medicine Lodge Creek. Lake levels fell again between 8,000—5,500 cal yr BP (Schuman and Serravezza 2017), indicating a local return to arid conditions, which is supported by fluxes of fine-grained eolian sedimentation in Alm Shelter and other local rockshelters like Paintrock V, Eagle Shelter, and BA Cave (Finley 2008). The onset of moister late Holocene conditions following 5,500 cal yr BP (Schuman and Serrevezza 2017) is consistent with the prominence of coarse-grained sediments originating from the south debris fan.

Regional Comparisons

Because of the lack of precision and major overlap of luminescence ages, modeled ages of stratigraphic contacts, and modeled ages of grain-size analysis trends, it is difficult to precisely connect the Alm Shelter deposit to broader regional climatic patterns. However, distinct fine-grained sedimentation occurs at Alm Shelter in well-stratified deposits dating to the early Holocene, around 11,000-8,000 cal yr BP. This tracks well with analyses conducted at

other sites in the western Bighorn Mountains, including Medicine Lodge Creek, Laddie Creek, Paint Rock V, and other rockshelters in the surrounding canyons (Finley 2008; Frison and Walker 2007; Reider and Karlstrom 1987). Further away in the Bighorn Basin, sites like Dead Indian Creek seem to have increased aridity later in the Holocene, around 7,500-5,000 cal yr BP (Reider et al. 1988), which is consistent with the fall in regional lake levels during the middle Holocene from 8,000-5,000 years ago (Schuman and Serrevezza 2017).

This study also compares paleoenvironmental records from around the western United States (Figure 2), though the precision of these methods varies widely. Figure 7 demonstrates periods of marked aridity using lake cores, wet meadow cores, and dune records compared against Alm Shelters luminescence ages and modeled ages of fine-grained deposits based on the grain-size analysis. Wyoming sites, outlined in the center, demonstrate some overlap between aridity identified at other sites and fine-grained deposits at Alm Shelter. Dune activation at the Killpecker Dunes in the Green River Basin to the south of the Bighorn Basin occurred at the transition from the Pleistocene into the early Holocene, around 11,000 cal yr BP, corresponding with increased eolian sedimentation at Alm Shelter (Ahlbrandt et al. 1983; Mayer and Mahan 2004). Lake of the Woods also demonstrates decreases in effective moisture during the Pleistocene-Holocene transition (Shuman et al. 2010). The Ferris and Casper Dunes were both active in the early Holocene, around 8,500 cal yr BP (Halfen et al. 2010; Stokes and Gaylord 1993). A second drop in effective moisture at Lake of the Woods occurred at 7,590 ± 1,450 cal yr BP, around the same time that Buckbean Fen and Sherd Lake experienced increased temperatures (Shuman 2012). Killpecker Dunes, Ferris Dunes, Casper Dunes, and Lake of the Woods experienced additional periods of aridity into the middle and late Holocene.

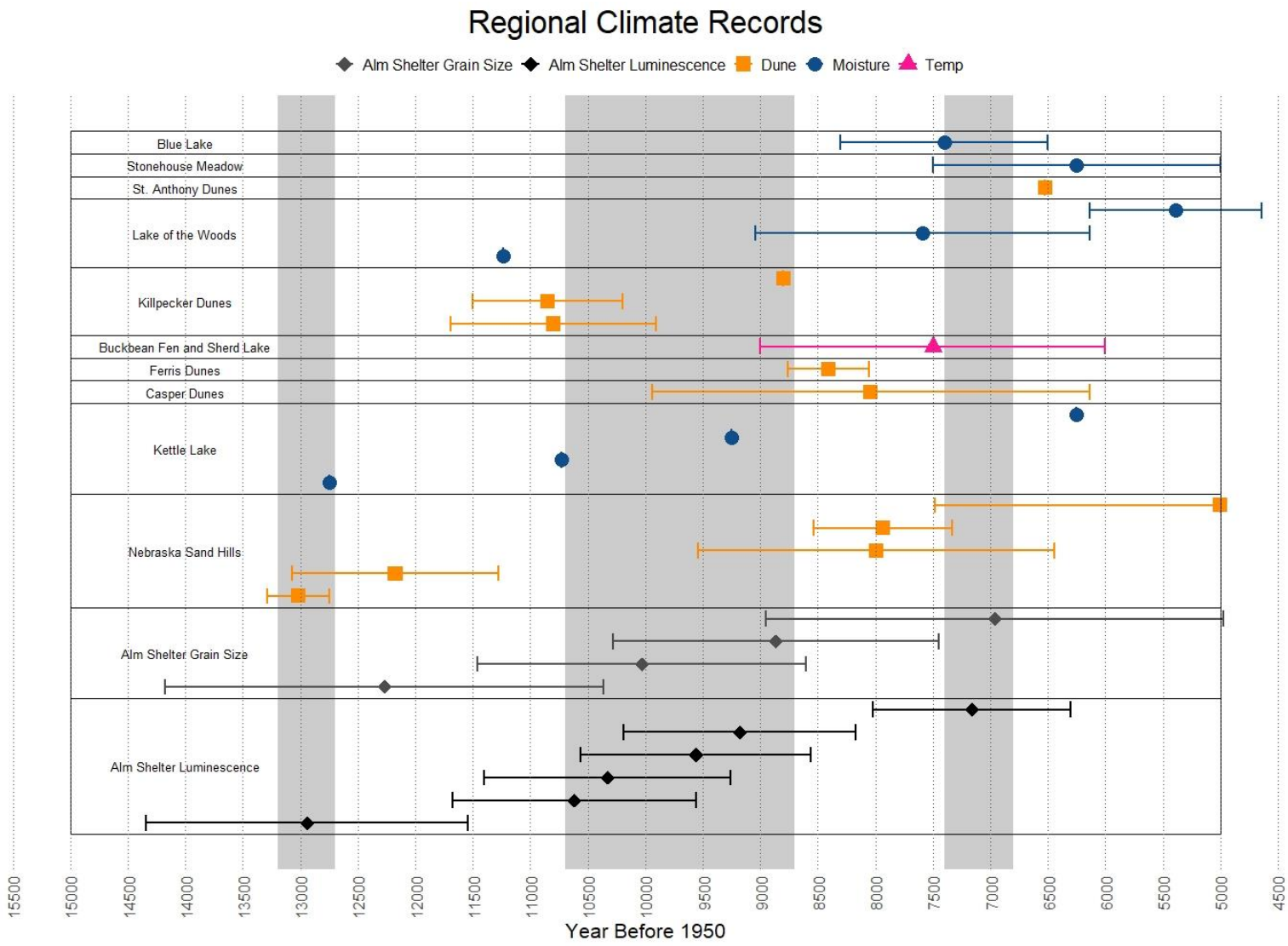

Figure 7. Comparison of eolian events with documented aridity events in the western United States.

Outside of Wyoming, decreased effective moisture occurred in the late Pleistocene at the Nebraska Sand Hills and Kettle Lake around 13,000-12,000 cal yr BP, overlapping with fine-grained deposits at Alm Shelter (Ahlbrant et al. 1983; Grimm et al. 2011; Loope et al. 1995; Miao et al. 2007; Stokes and Swinehart 1997). The Nebraska Sand Hills activated a number of times throughout the Holocene, notably at 8,000 cal yr BP and again at 6,000 cal yr BP, overlapping with eolian sedimentation at Alm Shelter. In addition to this, Kettle Lake experienced drops in effective moisture at 10,700 cal yr BP, 9,250 cal yr BP, and 6,250 cal yr BP, which correspond to multiple pulses of eolian sediments from Alm Shelter, and at 4,440 cal yr BP (Grimm et al. 2011). Other sites appear to have aridity events during the early to middle Holocene, like Blue Lake, Stonehouse Meadow, and the St. Anthony Dunes to the west of Alm Shelter (Louderback and Rhode 2009; Mensing et al. 2013; Rich et al. 2015). The earliest ages from these sites, between 8,000-6,000 cal yr BP, overlap with eolian deposits at Alm Shelter. As the luminescence record only extends to the early Holocene, later periods of aridity and increased temperature at other locations cannot be compared in this study. Because these other records track specific markers for aridity as well as temperature increases, the correlations indicated here demonstrate that some of the fine-grained deposits at Alm Shelter are likely due eolian sedimentation during periods of increased aridity.

Analytical Limitations

Interpretation of the Alm Shelter stratigraphy is limited by imprecision of age constraints using the selected luminescence dating methods, which have error terms (2-sigma) in excess of 1,000 years. This inherent lack of precision is translated into the OxCal age-depth model, which

shows a further dissolution of precision that ultimately limits the interpretive power of Alm Shelter in a local and regional environmental context. Another limitation of the methods used here is the presentation of luminescence with OxCal. Luminescence ages are traditionally presented in ka to prevent confusion related to BP values. However, OxCal is a program designed for radiocarbon ages, and therefore no option exists to present data in ka.

To trace regional climatic events accurately and precisely, it is necessary to develop a refined model with additional ages and increased precision. Additional luminescence ages from upper strata may not be effective, as human occupation during the middle and late Holocene may have affected the integrity of these deposits, evidenced by decreased definition of stratigraphic boundaries. Refining the model requires additional geochronological methods, including AMS ages spanning the Holocene deposits, and further incorporation of both the grain-size of Finley (2008) and this study, as well as potentially running grain-size analysis on the luminescence ages themselves. Other ways of constraining the large error margins of the luminescence ages includes using an age model, rather than an age-depth model, and incorporation of high-precision radiocarbon ages. With this additional level of precision, using the age-depth model to create modeled ages for individual grain-size samples becomes possible, as the grain-size samples span the entire deposit through the late Holocene. This will present a refined climatic chronology of Alm Shelter through the connection of modeled ages to specific depths and sediment textures, providing more precise information to compare to regional climate studies. Though the occupational history of Alm Shelter is not discussed here, this study also has implications for informing future studies of subsistence and settlement patterns of Bighorn Basin cultural groups during periods of variable climate and xeric conditions, as well as the potential for addressing larger questions of human movement and paleodemographics during widespread drought.

Conclusions

Alm Shelter is one of the most important rockshelters in the Bighorn Basin because of its relatively complete sequence of late Pleistocene and Holocene geoarchaeological deposits. Although rockshelters are notoriously singular in the style and span of depositional events that contain archaeological records (Woodward and Goldberg 2001), often preserving only pieces of the complete geoarchaeological sequence, Alm Shelter is an essential comparative key for the Bighorn Basin because of its relatively complete record. It is also important because it adds to the body of regional rockshelters that demonstrate the presence of viable stratigraphic deposits during the earliest occupations of North America beginning 13,600 cal yr BP, a vital piece of baseline information when discussing larger patterns of paleodemographics (Finley 2008; Holliday 2015; Wright 2011). Abrupt climate events can disrupt populations dramatically, forcing populations to adapt or redistribute across the landscape, and forthcoming studies address paleodemography and site use at Alm Shelter (Kelly et al. 2013). The long late Pleistocene and Holocene depositional sequence is an important archive of geomorphic linkages to environmental change. The stratigraphic analysis, luminescence ages, and an age-depth model from Alm Shelter indicates a shifting late Pleistocene and Holocene climate, marked by significant sediment availability during the deglaciation of the Bighorn Mountains in the late Pleistocene, followed by fluctuations of colluvial and eolian sedimentation through the Holocene. The history of site formation at Alm Shelter agrees broadly with local and regional

environmental changes that point to fluctuating moisture conditions through the early and middle Holocene, although this record based on OSL ages alone is limited in its precision. This environmental data compared to other regional climate studies demonstrates some correlations with increased aridity and temperatures at other sites across the western United States, indicating that some of the fine-grained deposits at Alm Shelter are likely related to periods of increased aridity that may be sub-continental in scale. Addressing the hypothesized presence of centennial-scale aridity events, this model fails to provide high precision information to constrain these events to a single century. Although promising, the low precision of the reconstruction indicates the need for a more refined chronology using radiocarbon ages as research at Alm Shelter moves forward toward a master site formation and use model.

References Cited

Ahlbrandt, Thomas S., James B. Swinehart, and David G. Maroney

1983 The Dynamic Holocene Dune Fields of the Great Plains and Rocky Mountain Basins, USA. In *Eolian Sediments and Processes*, edited by Michael E. Brookfield and Thomas S. Ahlbrandt, pp. 379–406. Elsevier, Amsterdam.

Aitken, Martin J.

1998 Prologue and 1: Basic Notions: Luminescence. In *An Introduction to Optical Dating*, pp. 1–36. Oxford University Press, Oxford.

Albanese, John P., and George C. Frison

1995 Cultural and Landscape Change During the Middle Holocene, Rocky Mountain Area, Wyoming and Montana. *Archaeological Geology of the Archaic Period in North America*:1–20.

Anderson, Derek T.

2007 Prehistoric Rockshelter Utilization in the Paint Rock Canyon Archaeological Landscape District. Master's thesis, Department of Anthropology, University of Wyoming, Laramie.

Auclair, Marie, Martin Lamothe, and Sebastien Huot

2003 Measurement of Anomalous Fading for Feldspar IRSL Using SAR. *Radiation Measurements* 37:487–492.

Bliss, Wesley L.

1950 Birdshead Cave, a Stratified Site in Wind River Basin. *American Antiquity* 15:187–196.

Bøtter-Jensen, Lars, Enver Bulur, Geoff A. T. Duller, and Andrew S. Murray

1999 Advances in Luminescence Measurement Systems. *Radiation Measurements* 32:523–528.

Boyd, Donald W.

1993 Paleozoic History of Wyoming. In *Geology of Wyoming*, edited by Arthur W. Snoke, James R. Steidtmann and Sheila. M Roberts, pp 164-187. Wyoming State Geological Survey, Laramie.

Bradley, Raymond S.

1999 *Paleoclimatology*. 2nd ed. Harcourt Academic Press, San Diego.

Bronk Ramsey, Christopher

2008 Deposition Models for Chronological Records. *Quaternary Science Reviews* 27:42–60.

Bronk Ramsey, Christopher

2009 Bayesian Analysis of Radiocarbon Dates. *Radiocarbon* 51:337–360.

Bronk Ramsey, Christopher, and Sharen Lee

2013 Recent and Planned Developments of the Program OxCal. *Radiocarbon* 55:720–730.

Brown, William G.

1993 Structural Style of Laramide Basement-Cored Uplifts and Associated Folds. In *Geology of Wyoming*, edited by Arthur W. Snoke, James R. Steidtmann and Sheila. M Roberts, pp 312-373. Wyoming State Geological Survey, Laramie.

Bullard, Joanna E., and Ian Livingstone

2002 Interactions Between Aeolian and Fluvial Systems in Dryland Environments. *Area* 34:8–16.

Busacca, Alan J., James E. Begét, Helaine W. Markewich, Daniel R. Muhs, Nicholas Lancaster, and Mark R. Sweeney

2003 Eolian Sediments. *Developments in Quaternary Science* 1:275–309.

Clarke, Michèle L., and Helen M. Rendell

1998 Climate Change Impacts on Sand Supply and the Formation of Desert Sand Dunes in the South-West U.S.A. *Journal of Arid Environments* 39:517–531.

Byers, David A., and Andrew Ugan

2005 Should We Expect Large Game Specialization in the Late Pleistocene? An Optimal Foraging Perspective on Early Paleoindian Prey Choice. *Journal of Archaeological Science* 32:1624–1640.

Clarkson, Chris, Zenobia Jacobs, Ben Marwick, Richard Fullagar, Lynley Wallis, Mike Smith, Richard G. Roberts, Elspeth Hayes, Kelsey Lowe, Xavier Carah, S. Anna Florin, Jessica McNeil, Delyth Cox, Lee J. Arnold, Quan Hua, Jillian Huntley, Helen E.A. Brand, Tiina Manne, Andrew Fairbairn, James Shulmeister, Lindsey Lyle, Makiah Salinas, Mara Page, Kate Connell, Gayoung Park, Kasih Norman, Tessa Murphy, and Colin Pardoe

2017 Human occupation of northern Australia by 65,000 years ago. Nature 547:306–310.

Craib, Alexander, Madeline Mackie, Spencer Pelton, Judson Byrd Finley, Erick N. Robinson, and Robert L. Kelly

2019 The Effects of Population and Climate Change on Site Use at Alm Shelter, Bighorn County, Wyoming: Preliminary Results.

Davis, Loren G., David B. Madsen, Lorena Becerra-Valdivia, Thomas Higham, David A. Sisson, Sarah M Skinner, Daniel Stueber, Alexander J. Nyers, Amanda Keen-Zebert, Christina Neudorf, Melissa Cheyney, Masami Izuho, Fumie Iizuka, Samuel R. Burns, Clinton W. Epps, Samuel C. Willis, and Ian Buvit

2019 Late Upper Paleolithic Occupation at Cooper's Ferry, Idaho, USA, ~16,000 Years Ago. *Science* 365:891–897.

Dean, Walter E., Thomas S. Ahlbrandt, Roger Y. Anderson, and J. Platt Bradbury

1996 Regional Aridity in North America During the Middle Holocene. *Holocene* 6:145–155.

Douka, Katerina, Zenobia Jacobs, Christine Lane, Rainer Grün, Lucy Farr, Chris Hunt, Robyn H. Inglis, Tim Reynolds, Paul Albert, Maxime Aubert, Victoria Cullen, Evan Hill, Leslie Kinsley, Richard G. Roberts, Emma L. Tomlinson, Sabine Wulf, and Graeme Barker

2014 The Chronostratigraphy of the Haua Fteah Cave (Cyrenaica, northeast Libya). *Journal of Human Evolution* 66:39–63.

Fenneman, Nevin Melancthon

1931 *Physiography of Western United States.* University of Michigan Press, Ann Arbor.

Ferbrache, Caleb E.

2019 Finding the Time: Age-Depth Models in Rockshelters and Their Paleoenvironmental Implications. Master's thesis, Department of Sociology, Social Work and Anthropology, Utah State University, Logan.

Finley, Judson Byrd

2007 Stratigraphy, Sedimentology and Geomorphology. In *Medicine Lodge Creek: Holocene Archaeology of the Eastern Big Horn Basin, Wyoming*, edited by George C. Frison and Danny N. Walker, pp. 131-152. Clovis Press, Phoenix.

Finley, Judson Byrd

2008 Rockshelter Formation Processes, Late Quaternary Environmental Change, and Hunter-Gatherer Subsistence in the Bighorn Mountains, Wyoming. PhD Dissertation, Department of Anthropology, Washington State University, Pullman.

Finley, Judson Byrd

2016 Late Holocene Geoarchaeology in the Bighorn Basin, Wyoming. In *Stones, Bones, and Profiles: Exploring Archaeological Context, Early American Hunter-Gatherers, and Bison*, edited by Marcel Kornfeld and Bruce B. Huckell, pp. 259–288. University of Colorado Press, Boulder.

Finley, Judson Byrd, Carlie J. Ideker, and Tammy Rittenour

2017 Single-Grain Optically Stimulated Luminescence Ages of Brownware Pottery in the Middle Rocky Mountains and the Spread of Numic Ceramic Technology. *American Antiquity* 82:761–780.

Finley, Judson Byrd, Erick Robinson, R. Justin DeRose, and Elizabeth Hora

2020 Multidecadal Climate Variability and the Florescence of Fremont Societies in Eastern Utah. *American Antiquity* 85:93-112.

Finley, Judson Byrd, Marcel Kornfeld, Brian N. Andrews, George C. Frison, Chris C. Finley, and Michael T. Bies

2005 Rockshelter Archaeology and Geoarchaeology in the Bighorn Mountains, Wyoming. *Plains Anthropologist* 50:227–248.

Forman, Steven L., Liliana Marín, James Pierson, Jeaneth Gómez, Gifford H. Miller, and Robert S. Webb

2005 Aeolian Sand Depositional Records from Western Nebraska: Landscape Response to Droughts in the Past 1500 Years. *Holocene* 15:973–981.

Francis, Julie E., and Lawrence L. Loendorf

2002 *Ancient Visions: Petroglyphs and Pictographs of the Wind River and Bighorn Country, Wyoming and Montana.* University of Utah Press, Salt Lake City.

Frison, George C.

1962 Wedding of the Waters Cave, 48HO304, A Stratified Site in the Big Horn Basin of Northern Wyoming. *Plains Anthropologist* 7:246–265.

Frison, George C.

1965 Spring Creek Cave, Wyoming. *American Antiquity* 31:81–94.

Frison, George C.

1968 Daugherty Cave, Wyoming. *Plains Anthropologist* 13:253–295.

Frison, George C.

1973 Early Period Marginal Cultural Groups in Northern Wyoming. *Plains Anthropologist* 18:300–312.

Frison, George C.

1993 North American High Plains Paleo-Indian Hunting Strategies and Weaponry Assemblages. In *From Kostenki to Clovis*, edited by Olga Soffer and Nikolai Dmitrievich Praslov. Springer, New York.

Frison, George C.

1997 The Foothill-Mountain Late Paleoindian an Early Plains Archaic Chronology and Subsistence. In *Changing Perspective of the Archaic on the Northwest Plains and Rocky Mountains*, edited by Mary Lou Larson and Julie E. Francis, pp. 84–104. University of South Dakota Press, Vermillion.

Frison, George C.

2007 Background of Great Plains and Rocky Mountain Archaeology. In *Medicine Lodge Creek: Holocene Archaeology of the Eastern Big Horn Basin, Wyoming*, edited by George C. Frison and Danny N. Walker, pp. 1–11. Clovis Press, Phoenix.

Frison, George C., and Bruce A. Bradley

1980 *Folsom Tools and Technology at the Hanson Site, Wyoming.* University of New Mexico Press, Albuquerque.

Frison, George C., and Danny N. Walker

2007 The Medicine Lodge Creek Archaeological Project. In *Medicine Lodge Creek: Holocene Archaeology of the Eastern Big Horn Basin, Wyoming*, edited by George C. Frison and Danny N. Walker, pp. 12–32. Clovis Press, Phoenix.

Frison, George C., and Donald C. Grey

1980 Pryor Stemmed: A Specialized Late Paleo-Indian Ecological Adaptation. *Plains Anthropologist* 25:27–46.

Frison, George C., and Marion Huseas

1968 Leigh Cave, Wyoming: Site 48 WA304. *The Wyoming Archaeologist* 11:20–33.

Frison, George C., and Lawrence C. Todd

1986 *The Colby Mammoth Site: Taphonomy and Archaeology of a Clovis Kill in Northern Wyoming*. University of New Mexico Press, Albuquerque.

Frison, George C., and Lawrence C. Todd (editors)

1987 *The Horner Site.* Academic Press, Cambridge.

Frison, George C., Ron L. Andrews, James M. Adovasio, Ronald C. Carlisle, and Robert Edgar

1986 A Late Paleoindian Animal Trapping Net from Northern Wyoming. *American Antiquity* 51:352–361.

Galbraith, Rex F., and Richard G. Roberts

2012 Statistical Aspects of Equivalent Dose and Error Calculation and Display in OSL Dating: An Overview and Some Recommendations. *Quaternary Geochronology* 11:1–27.

Gliganic, Luke A., Zenobia Jacobs, Richard G. Roberts, Manuel Domínguez-Rodrigo, and Audax Z.P. Mabulla

2012 New Ages for Middle and Later Stone Age Deposits at Mumba Rockshelter, Tanzania: Optically Stimulated Luminescence Dating of Quartz and Feldspar Grains. *Journal of Human Evolution* 62:533–547.

Grimm, Eric C., Joseph J. Donovan, and Kendrick J. Brown

2011 A High-Resolution Record of Climate Variability and Landscape Response from Kettle Lake, Northern Great Plains, North America. *Quaternary Science Reviews* 30:2626–2650.

Guérin, Guillaume, Nicolas Mercier, and Grzegorz Adamiec

2011 Dose-Rate Conversion Factors: Update. *Ancient TL* 29:5–8.

Halfen, Alan F., Glen G. Fredlund, and Shannon A. Mahan

2010 Holocene Stratigraphy and Chronology of the Casper Dune Field, Casper, Wyoming, USA. *Holocene* 20:773–783.

Haslett, John, and Andrew Parnell

2008 A Simple Monotone Process with Application to Radiocarbon-Dated Depth Chronologies. *Journal of the Royal Statistical Society. Series C: Applied Statistics* 57:399–418.

Huckleberry, Gary, and Tammy Rittenour

2014 Combining Radiocarbon and Single-Grain Optically Stimulated Luminescence Methods to Accurately Date Pre-Ceramic Irrigation Canals, Tucson, Arizona. *Journal of Archaeological Scienc*e 41:156–170.

Hugenholtz, Christopher H., and Steven A. Wolfe

2005 Biogeomorphic Model of Dunefield Activation and Stabilization on the Northern Great Plains. *Geomorphology* 70:53–70.

Huntley, David J., Dorothy I. Godfrey-Smith, and Michael L.W. Thewalt

1985 Optical Dating of Sediments. *Nature* 313:105–107.

Huntley, David J., and Martin Lamothe

2001 Ubiquity of Anomalous Fading in K-Feldspars and the Measurement and Correction for it in Optical Dating. *Canadian Journal of Earth Sciences* 38:1093–1106.

Husted, Wilfred M.

1964 *Publications in Salvage Archaeology, 12: Bighorn Canyon Archeology*. Publications in Salvage Archaeology vol. 12. Smithsonian Institution, Lincoln, Nebraska.

Kelly, Robert L., Todd A. Surovell, Bryan N. Shuman, and Geoffrey M. Smith

2013 A continuous climatic impact on Holocene Human Population in the Rocky Mountains. *Proceedings of the National Academy of Sciences* 110:443–447.

Kelly, Robert L., and Lawrence C. Todd

1988 Coming into the Country: Early Paleoindian Hunting and Mobility. *American Antiquity* 53:231–244.

Knight, Dennis H.

1994 *Mountains and Plains: The Ecology of Wyoming Landscapes.* Yale University Press, New Haven.

Knight, Melanie, David S.G. Thomas, and Giles F.S. Wiggs

2004 Challenges of Calculating Dunefield Mobility over the 21st Century. Geomorphology 59:197–213.

Knox, James C.

1972 Valley Alluviation in Southwestern Wisconsin. *Annals of the Association of American Geographers* 62:401–410.

Kornfeld, Marcel

2007 Rockshelter of the Middle Rocky Mountains: 70 Years of Research. In *On Shelter's Ledge: Histories, Theories and Methods of Rockshelter Research*, edited by Marcel Kornfeld, Sergey A Vasil'ev, and Laura Miotti, pp. 51–61. Hadrian Books, Oxford.

Kornfeld, Marcel, George C. Frison, and Mary Lou Larson

2010 *Prehistoric Hunter-Gatherers of the High Plains and Rockies.* Left Coast Press, Walnut Creek, California.

Larson, Mary Lou

1992 Site Formation Processes in the Cody and Early Plains Archaic Levels at the Laddie Creek Site, Wyoming. *Geoarchaeology: An International Journal* 7:103–120.

Loope, David B., James B. Swinehart, and Jon P. Mason

1995 Dune-Dammed Palaeovalleys of the Nebraska Sand Hills: Intrinsic Versus Climatic Controls on the Accumulation of Lake and Marsh Sediments. *Geological Society of America Bulletin* 107:396–406.

Licciardi, Joseph M., and Kenneth L. Pierce

2008 Cosmogenic Exposure-Age Chronologies of Pinedale and Bull Lake Glaciations in Greater Yellowstone and the Teton Range, USA. *Quaternary Science Reviews* 27:814–831.

Louderback, Lisbeth A., and David E. Rhode

2009 15,000 Years of Vegetation Change in the Bonneville Basin: The Blue Lake Pollen Record. *Quaternary Science Reviews* 28:308–326.

Lyford, Mark E., Julio L. Betancourt, and Stephen T. Jackson

2002 Holocene Vegetation and Climate History of the Northern Bighorn Basin, Southern Montana. *Quaternary Research* 58:171-181.

Mejdahl, Vagn

1979 Thermoluminescence Dating: Beta-Dose Attenuation in Quartz Grains. *Archaeometry* 21:61–72.

Malvern Instruments

2007 *Mastersizer 2000 User Manual*. Malvern Instruments, Malvern, UK.

Martner, Brooks E.

1986 *Wyoming Climate Atlas.* University of Nebraska Press, Lincoln.

Mayer, James H., and Shannon A. Mahan

2004 Late Quaternary Stratigraphy and Geochronology of the Western Killpecker Dunes, Wyoming, USA. *Quaternary Research* 61:72–84.

Mensing, Scott A., Saxon E. Sharpe, Irene Tunno, Don W. Sada, Jim M. Thomas, Scott Starratt, and Jeremy Smith

2013 The Late Holocene Dry Period: Multiproxy evidence for an Extended Drought Between 2800 and 1850calyr BP Across the Central Great Basin, USA. *Quaternary Science Reviews* 78:266–282.

Miao, Xiaodong, Joseph A. Mason, James B. Swinehart, David B. Loope, Paul R. Hanson, Ronald J. Goble, and Xiaodong Liu

2007 A 10,000 Year Record of Dune Activity, Dust Storms, and Severe Drought in the Central Great Plains. *Geology* 35:119–122.

Millard, Andrew

2004 Taking Bayes Beyond Radiocarbon: Bayesian Approaches to Some Other Chronometric Methods. In *Tools for Constructing Chronologies*, edited by Caitlin E Buck and Andrew Millard, pp. 231–248. Springer, London.

Minckley, Thomas A., Mark Clementz, Marcel Kornfeld, Mary Lou Larson, and Judson Byrd Finley

2021 Late Pleistocene Environments of the Bighorn Basin, Wyoming-Montana, USA. *Quaternary Research* 99:128–141.

Mitchell, Val L.

1976 The Regionalization of Climate in the Western United States. In *Journal of Applied Meteorology* 15:920-927.

Murray, Andrew S., and Jon M. Olley

2002 Precision and Accuracy in the Optically Stimulated Luminescence Dating of Sedimentary Quartz: A Status Review. *Geochronometria* 21:1–16.

Murray, Andrew S., and Ann G. Wintle

2000 Luminescence Dating of Quartz Using an Improved Single-Aliquot Regenerative-Dose Protocol. *Radiation Measurements* 32:57–73.

National Research Council

2006 *Surface Temperature Reconstructions for the Last 2,000 Years*. The National Academies Press, Washington, D.C.

Nelson, Michelle S., Harrison J. Gray, Jack A. Johnson, Tammy M. Rittenour, James K. Feathers, and Shannon A. Mahan

2015 User Guide for Luminescence Sampling in Archaeological and Geological Contexts. *Advances in Archaeological Practice* 3:166–177.

Nicholson, Christopher, Thomas A. Minckley, and Jacqueline J. Shinker

2019 Validating CCSM3 Paleoclimate Data Using Pollen-Based Reconstruction in the Intermountain West. *Quaternary Science Reviews* 222:105911.

Ostahowski, Brian E., and Robert L. Kelly

2014 Alm Rockshelter Lithic Debitage Analysis: Implications for Hunter-Gatherer Mobility Strategies in the Big Horn Mountains, Wyoming. In *Lithics in the West*, edited by Douglas H. MacDonald, William Jr. Andrefsky, and Pei-Lia Yu, pp. 118–139. University of Montana Press, Missoula.

Parnell, Andrew C., Caitlin E. Buck, and Thinh K. Doan

2011 A Review of Statistical Chronology Models for High-Resolution, Proxy-Based Holocene Palaeoenvironmental Reconstruction. *Quaternary Science Reviews* 30:2948–2960.

Picard, M. Dane

1993 The Early Mesozoic History of Wyoming. In *Geology of Wyoming*, edited by Arthur W. Snoke, James R. Steidtmann and Sheila. M. Roberts, pp 210-248. Geological Survey of Wyoming, Laramie.

Pierce, William G.

1997 Geologic Map of the Cody 1 Degree X 2 Degree Quadrangle, Northwestern Wyoming. Electronic document, https://ngmdb.usgs.gov/Prodesc/proddesc_13047.htm, accessed January 23, 2020.

Reider, Richard G., Gary A. Huckleberry, and George C. Frison

1988 Soil Evidence for Postglacial Forest-Grassland Fluctuation in the Absaroka Mountains of Northwestern Wyoming, USA. *Arctic & Alpine Research* 20:188–198.

Reider, Richard G., and Eric T. Karlstrom

1987 Soils and Stratigraphy of the Laddie Creek Site (48BH345), an Altithermal-Age Occupation in the Big Horn Mountains. *Geoarchaeology: An International Journal* 2:29–47.

Rich, Julie, Tammy M. Rittenour, Michelle S. Nelson, and Justin Owen

2015 OSL Chronology of Middle to Late Holocene Aeolian Activity in the St. Anthony Dune Field, Southeastern Idaho, USA. *Quaternary International* 362:77–86.

Rittenour, Tammy M., Larry L. Coats, and Duncan Metcalfe

2015 Investigation of Late and Post-Fremont Alluvial Stratigraphy of Range Creek, East-Central Utah: Use of OSL when Radiocarbon Fails. *Quaternary International* 362:63–76.

Robbins, Lawrence, Alec C. Campbell, George A. Brook, Michael L. Murphy, and Robert K. Hitchcock

2012 The Antiquity of the Bow and Arrow in the Kalahari Desert: Bone Points from White Paintings Rock Shelter, Botswana. *Journal of African Archaeology* 10:1612–1651.

Salisbury, Rollin D., and Eliot Blackwelder

1903 Glaciation in the Bighorn Mountains. *The Journal of Geology* 11:216–223.

Sando, William J.

1974 Ancient Solution Phenomena in the Madison Limestone (Mississippian) of North-Central Wyoming. *Journal of Research of the US Geological Survey* 2:133-141.

Sando, William J.

1988 Madison Limestone (Mississippian) Paleokarst: A Geological Synthesis. In *Paleokarst*, edited by Kyger C. Lohmann, Philip W. Choquette and Noel P. James, pp 256-277. Springer-Verlag Press, New York.

Shuman, Bryan N.

2012 Recent Wyoming Temperature Trends, Their Drivers, and Impacts in a 14,000-Year Context. *Climatic Change* 112:429–447.

Shuman, Bryan N., and Jeremiah Marsicek

2016 The Structure of Holocene Climate Change in Mid-Latitude North America. *Quaternary Science Reviews* 141:38–51.

Shuman, Bryan N., and Marc Serravezza

2017 Patterns of Hydroclimatic Change in the Rocky Mountains and Surrounding Regions Since the Last Glacial Maximum. *Quaternary Science Reviews* 173:58–77.

Shuman, Bryan N., Paul Pribyl, Thomas A. Minckley, and Jacqueline J. Shinker

2010 Rapid Hydrologic Shifts and Prolonged Droughts in Rocky Mountain Headwaters During the Holocene. *Geophysical Research Letters* 37:1–5.

Soil Survey Staff

1999 *Soil Taxonomy: A Basic System of Soil Classification for Making and Interpreting Soil Surveys.* 2nd ed. Natural Resources Conservation Service. U.S. Department of Agriculture Handbook 436.

Steidtmann, James R.

1993 The Cretaceous Foreland Basin and its Sedimentary Record. In *Geology of Wyoming*, edited by Arthur W. Snoke, James R. Steidtmann and Sheila. M. Roberts, pp 250-271. Geological Survey of Wyoming, Laramie.

Stevens, Thomas, Simon J. Armitage, Huayu Lu, and David S.G. Thomas

2006 Sedimentation and Diagenesis of Chinese Loess: Implications for the Preservation of Continuous, High-Resolution Climate Records. *Geology* 34:849–852.

Stokes, Stephen, and David R. Gaylord

1993 Optical Dating of Holocene Dune Sands in the Ferris Dune Field, Wyoming. *Quaternary Research.*

Stokes, Stephen, and James B. Swinehart

1997 Middle- and Late-Holocene Dune Reactivation in the Nebraska Sand Hills, USA. *Holocene* 7:263–272.

Stuiver, Minze, Paula J. Reimer, and Ron W. Reimer

2021 CALIB 8.2. Electronic program. http://calib.org, accessed January 3, 2021.

Surovell, Todd A., Judson Byrd Finley, Geoffrey M. Smith, P. Jeffrey Brantingham, and Robert Kelly

2009 Correcting Temporal Frequency Distributions for Taphonomic Bias. *Journal of Archaeological Science* 36:1715–1724.

Sutherland, Peter W.

1976 *The Geomorphic History of Horsethief Cave, Bighorn Mountains, Wyoming.* University of Wyoming Press, Laramie.

Tate, Susan E., Richard S.B. Greene, Keith M. Scott, and Kenneth G. McQueen

2007 Recognition and Characterisation of the Aeolian Component in Soils in the Girilambone Region, North Western New South Wales, Australia. *Catena* 69:122–133.

Wallinga, Jakob, Andrew Murray, and Geoff Duller

2000 Underestimation of Equivalent Dose in Single-Aliquot Optical Dating of Feldspars Caused by Preheating. *Radiation Measurements* 32:691–695.

Warner, Kathryn, Mo Hamza, Anthony Oliver-Smith, Fabrice Renaud, and Alex Julca

2010 Climate Change, Environmental Degradation and Migration. *Natural Hazards* 55:689–715.

Wentworth, Chester K.

1922 A Scale of Grade and Class Terms for Clastic Sediments. *The Journal of Geology* 30:377-392.

Western Regional Climate Center

2021 Monthly Average Temperatures. Electronic Document, https://wrcc.dri.edu/Climate/comp_table_state_show.php?stype=temp_month_avg&sstate=wy&stitle=Monthly+Average+Temperatures&sparent=o-w, accessed January 23, 2021.

Wintle, Ann G., and Andrew S. Murray

2006 A Review of Quartz Optically Stimulated Luminescence Characteristics and Their Relevance in Single-Aliquot Regeneration Dating Protocols. *Radiation Measurements* 41:369–391.

Wolff, Eric W.

2007 When is the "present"? *Quaternary Science Reviews* 26:3023–3024.

Woodward, Jamie C., and Paul Goldberg

2001 The Sedimentary Records in Mediterranean Rockshelters and Caves: Archives of Environmental Change. *Geoarchaeology - An International Journal* 16:327–354.

Wright, David K.

2011 Frontier Animal Husbandry in the Northeast and East African Neolithic: A Multiproxy Paleoenvironmental and Paleodemographic Study. *Journal of Anthropological Research* 67:231–244.

Appendices

Appendix A: Granulometry

Table 5. Grain Size Results from Malvern Mastersizer 2000 Analysis.

Profile Sample	Median Depth	d (0.1)	d (0.5)	d (0.9)	% clay	%vfsilt	%fsilt	%msilt	%csilt	% vcsilt	%vfsand	%fsand	%msand	%csand	%> 1mm
10207	96.6	10.043	164.7968	522.9923	2.284138	2.468108	3.573409	4.384699	5.829727	9.642344	13.75756	20.3747	25.05626	12.62905	8.7
10208	96.72	4.165222	42.98478	223.6688	4.446127	4.725381	7.541753	10.54483	13.8828	18.21453	18.17733	13.63161	7.67044	1.165199	6.8
10209	96.95	3.090667	24.47889	68.02656	6.123726	6.09039	9.536145	13.53738	23.00387	28.12391	11.83981	0.91147	0.740556	0.092746	20.6
10210	97.15	2.963667	20.415	61.89744	6.391258	6.26186	9.78454	16.89768	26.51235	23.56671	8.35501	0.683885	0.721244	0.82547	18.1
10211	97.4	2.630778	21.66189	85.08189	7.198787	7.066181	11.07495	15.29407	19.05077	21.67261	14.09962	3.339075	0.691416	0.512519	26.9
10212	97.55	2.744556	21.66978	83.55711	6.960843	6.590019	10.2138	15.46912	22.08824	22.22372	10.41848	2.15686	1.826642	2.052282	43
10213	97.75	5.085889	56.13511	629.8016	4.045627	3.726162	5.969392	8.784451	13.06251	16.0453	12.5122	8.076104	10.98723	16.79103	72.7
10214	98.25	3.568333	29.95656	201.3636	5.58404	4.98489	7.831292	12.72671	19.13426	21.30029	13.93066	5.682906	4.411228	4.413718	51.2
10215	98.55	5.509444	37.48033	443.585	3.598878	3.401109	6.473127	11.51833	18.27788	20.99334	13.71769	6.151603	6.771052	9.09698	52.7
10216	98.67	6.491333	36.60467	353.7213	3.270762	2.717843	5.707487	11.90501	19.94754	22.43468	14.54728	6.509944	5.857024	7.102437	37.3
10217	98.72	4.760444	19.827	60.11056	5.182087	3.289664	7.031738	21.48034	33.56271	19.68061	4.528511	1.919587	1.565852	1.758901	14.8
10218	98.9	7.131444	31.41444	403.4972	3.186019	1.976932	5.672162	15.63657	22.34407	18.10468	11.4316	6.883002	6.63483	8.130128	46.5
10219	99.15	5.690111	38.30156	326.9909	3.788838	3.257751	5.723605	10.34277	18.65973	23.77062	15.70559	6.469657	5.659022	6.622413	65.4
10220	99.47	8.753667	47.39678	435.604	2.490014	2.04082	4.172199	8.659948	17.40572	23.16389	17.01104	8.612604	7.642017	8.801746	76.8
10222	99.67	6.398667	45.77322	385.0219	3.400411	2.978311	5.138009	9.090308	16.50109	21.41302	16.88192	9.422437	7.735648	7.438851	77.2
10223	97.9	2.452111	16.62433	70.89744	7.97722	6.889794	11.81445	19.95718	25.13568	16.40824	5.33303	2.465474	2.192535	1.8264	55.7

10224	98.07	3.941778	30.382	199.3159	5.165443	4.342278	7.285131	11.93816	19.67804	22.25422	13.27094	5.525719	4.751557	5.788516	43.1
10225	98.2	4.299222	27.05033	108.4193	4.99587	3.989952	7.338969	14.08985	23.83752	24.3026	12.63452	4.184567	2.69686	1.92929	34.2
10226	98.27	3.492556	25.44344	167.277	5.792054	4.978662	8.340879	14.78038	21.79928	19.96623	11.66128	5.065829	3.593539	4.021868	41.3
10227	98.3	4.208	35.60656	430.7346	4.931941	4.235025	6.833625	10.79642	18.02801	20.8752	12.85745	6.018885	6.664975	8.758473	41.8
10228	98.7	3.107	19.405	57.04911	6.546447	5.359349	9.449803	18.73653	29.33995	21.62495	5.440207	1.189335	1.15732	1.156117	12.1
10230	98.93	5.840889	45.00011	392.8897	3.733895	3.322654	5.11396	8.305804	16.17608	23.3701	17.65485	8.132056	6.24163	7.948967	53.2
10231	98.47	4.709778	40.99811	409.443	4.211855	4.006472	6.777405	10.46884	15.89562	19.69105	14.84477	8.170467	7.81115	8.122368	30.1

Appendix B: Luminescence

Table 6. Dose Rate Information.

USU num.	In-situ H_2O (%)[a]	Grain size (µm)	DR Sample[b]	K (%)[c]	Rb (ppm)[c]	Th (ppm)[c]	U (ppm)[c]	Cosmic[d] (Gy/kyr)
USU-3039	1.3	63-150	F (100%)	1.53±0.04	51.6±2.1	8.5±0.8	1.7±0.1	0.21±0.02
USU-3040	1.8	63-250	F (30%)	1.70±0.04	70.2±2.8	8.4±0.8	2.1±0.2	0.22±0.02
			M (10%)	0.14±0.01	5.3±0.2	0.7±0.1	1.0±0.1	
			C (30%)	0.05±0.01	1.9±0.1	0.2±0.01	1.0±0.1	
			B (30%)	0.09±0.01	1.5±0.6	0.1±0.01	1.1±0.1	
USU-3041	9.5	90-180	F (100%)	1.57±0.04	50.3±2.0	9.6±0.9	1.5±0.1	0.10 ± 0.01
USU-3042	13.9	75-150	F (45%)	1.51±0.04	52.2±2.1	9.3±0.8	1.8±0.1	0.10 ± 0.01
			M (10%)	0.68±0.02	22.4±0.9	2.3±0.2	1.7±0.1	
			C (45%)	0.09±0.002	2.8±0.1	0.3±0.03	0.8±0.1	
USU-3043	5.0	90-150	F (100%)	1.46±0.04	49.4±2.0	8.2±0.7	1.8±0.1	0.10 ± 0.01
USU-3044	3.2	63-250	F (55%)	1.60±0.04	40.8±1.6	4.2±0.4	1.5±0.1	0.11 ± 0.01
			M (25%)	0.27±0.01	5.3±0.2	0.6±0.1	0.8±0.1	
			C (20%)	0.14±0.004	2.8±0.1	0.3±0.02	0.7±0.1	
USU-3045	4.1	63-250	F (60%)	1.51±0.04	38.5±1.5	3.7±0.3	1.5±0.1	0.11±0.01
			M (30%)	0.31±0.01	4.8±0.2	0.5±0.05	1.0±0.1	
			C (10%)	0.19±0.005	4.0±0.2	0.4±0.03	0.8±0.1	

USU num.	In-situ H_2O (%)[a]	Grain size (µm)	DR Sample[b]	K (%)[c]	Rb (ppm)[c]	Th (ppm)[c]	U (ppm)[c]	Cosmic[d] (Gy/kyr)
USU-3046	2.6	63-250	F (50%)[e]	1.22±0.03	30.0±1.2	2.9±0.3	1.2±0.1	0.11±0.01
USU-3047	4.0	63-250	F (100%)	1.39±0.03	32.3±1.3	3.0±0.3	1.2±0.1	0.12±0.01
USU-3048	4.1	63-250	F (100%)	1.26±0.03	33.7±1.3	3.1±0.3	1.2±0.1	0.12±0.01
USU-3049	2.2	63-250	F (70%)	1.74±0.04	47.6±1.9	4.5±0.4	1.5±0.1	0.12±0.01
			M (20%)	0.45±0.01	10.5±0.4	1.3±0.1	1.0±0.1	
			C (10%)	0.12±0.003	2.4±0.1	0.3±0.02	0.7±0.1	

[a] For USU-3039:-3040 and USU-3043:-3048 5.0±2.0% used as moisture content over burial history. USU-3041 and USU-3042 uses 10.0±3.0%.

[b] Dose rate subsamples differentiated by grain size: <1.7 mm (fine, F), 1.7-16 mm (medium, M), 16-256 mm (coarse, C), and >256 mm (boulder, B). If more than 1 fraction is reported, the gamma dose rate is the weighted average of chemical concentrations based on mass for each fraction. Beta dose rate uses chemistry from fine fraction only.

[c] Radioelemental concentrations determined using ICP-MS and ICP-AES techniques; dose rate is derived from concentrations by conversion factors from Guérin et al. (2011).

[d] Cosmic DR reduced by 50% due to rock wall for USU-3041:USU-3049.

[e] Remaining 50% of contribution includes dose rate chemistry from USU-3045 F (45%) and M+C (5%).

Figure 8. Equivalent dose distributions, with probability density function, radial and overdispersion (OD) plots.

1. 48BH3457-8855, USU-3039 OSL

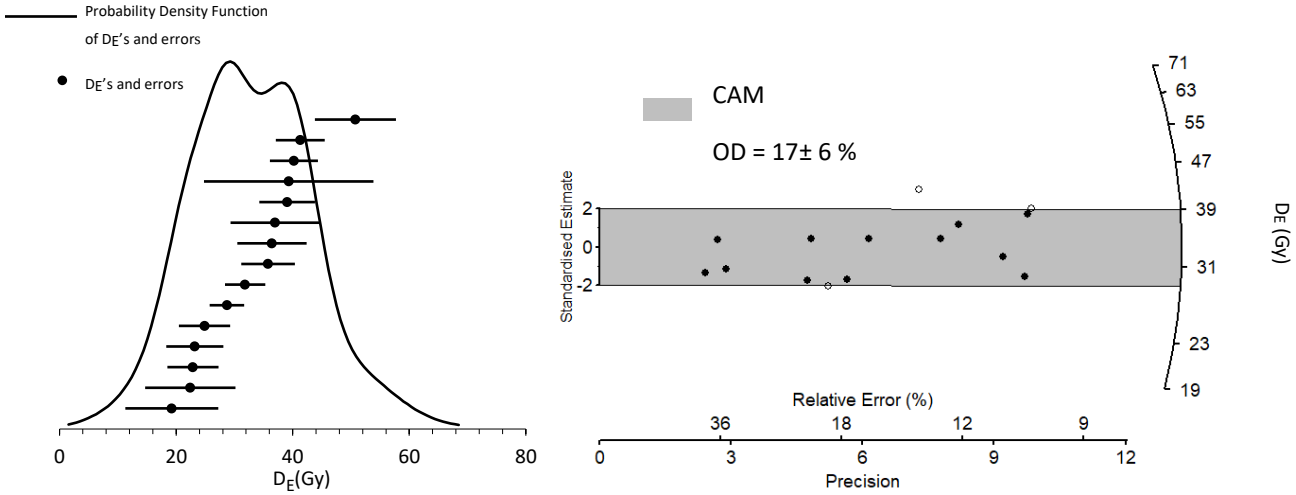

2. 48BH3457-8878, USU-3040 OSL

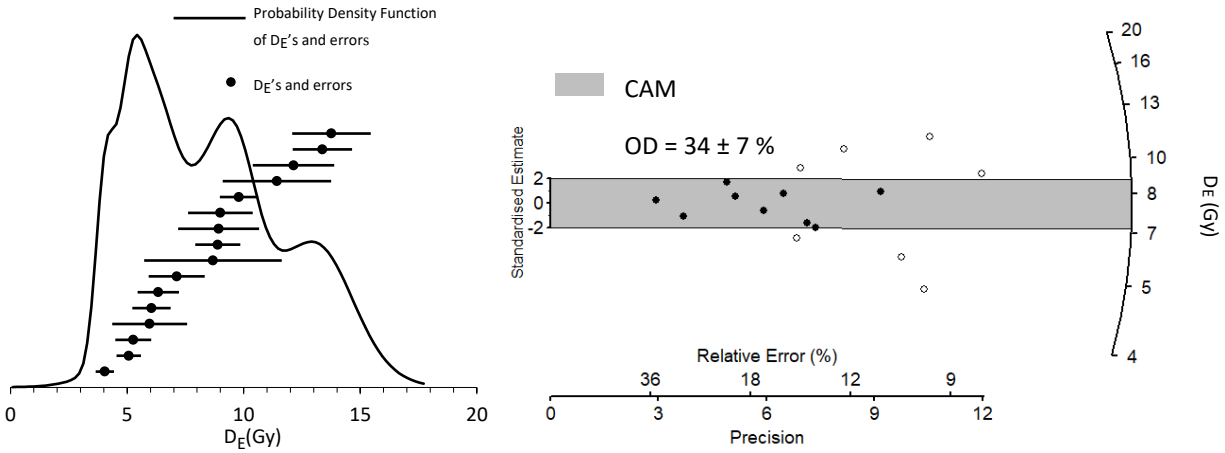

3. 48BH3457-2018-1, USU-3041 OSL

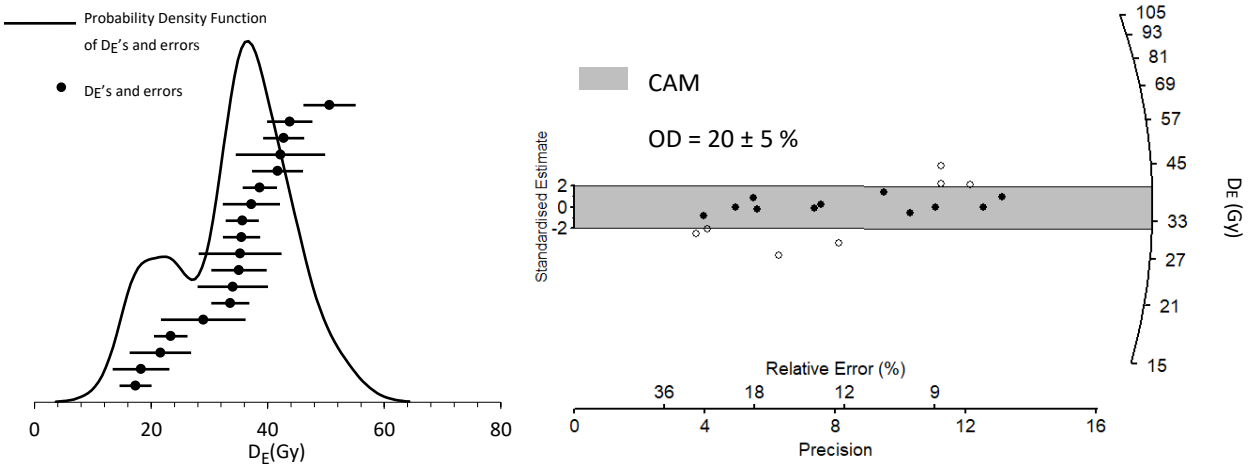

4. 48BH3457-2018-2, USU-3042 OSL

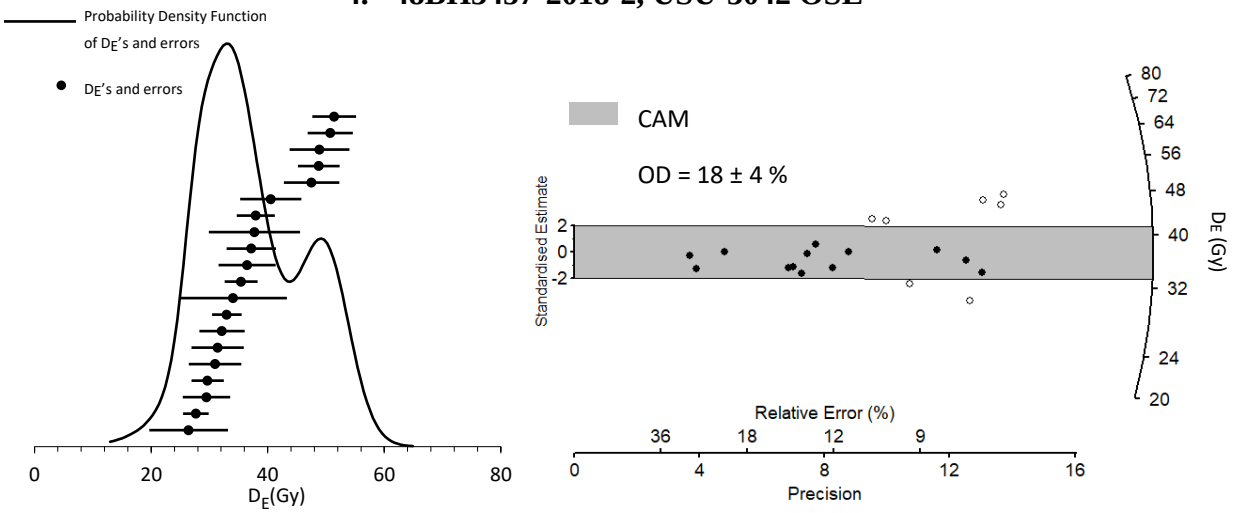

5. 48BH3457-2018-3, USU-3043 OSL

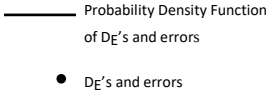

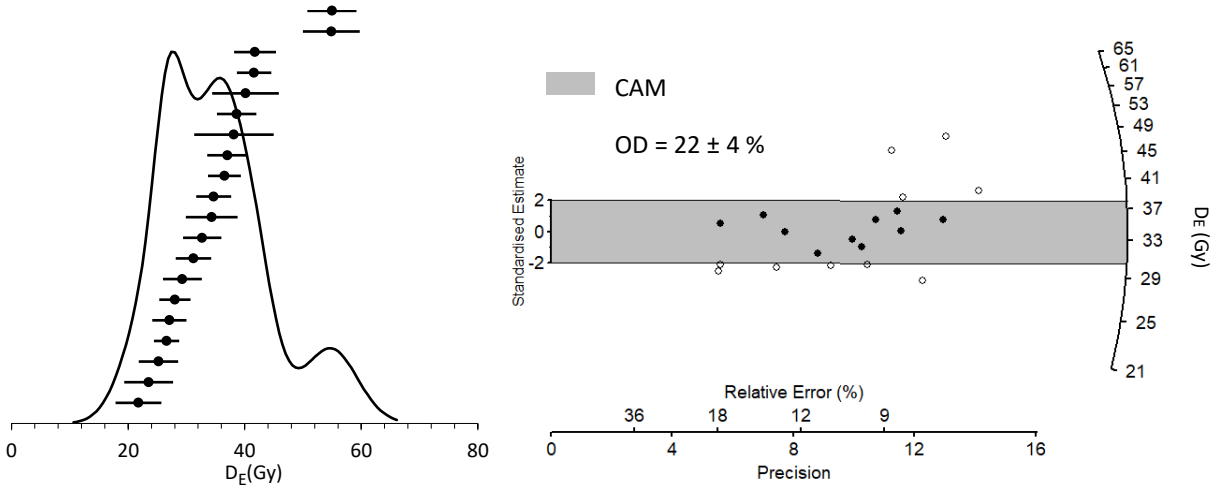

6. 48BH3457-2018-4, USU-3044 IRSL

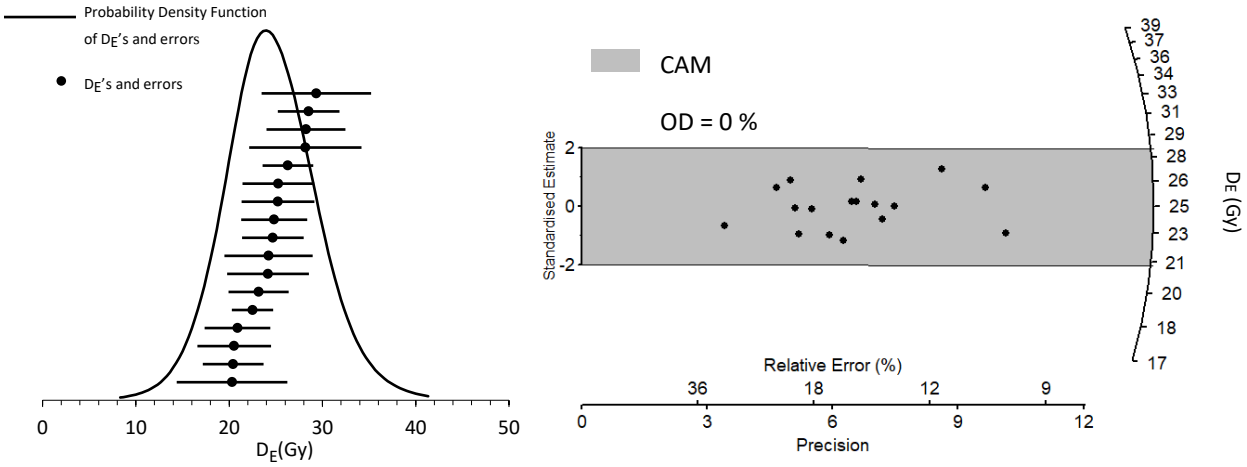

7. 48BH3457-2018-5, USU-3045 OSL

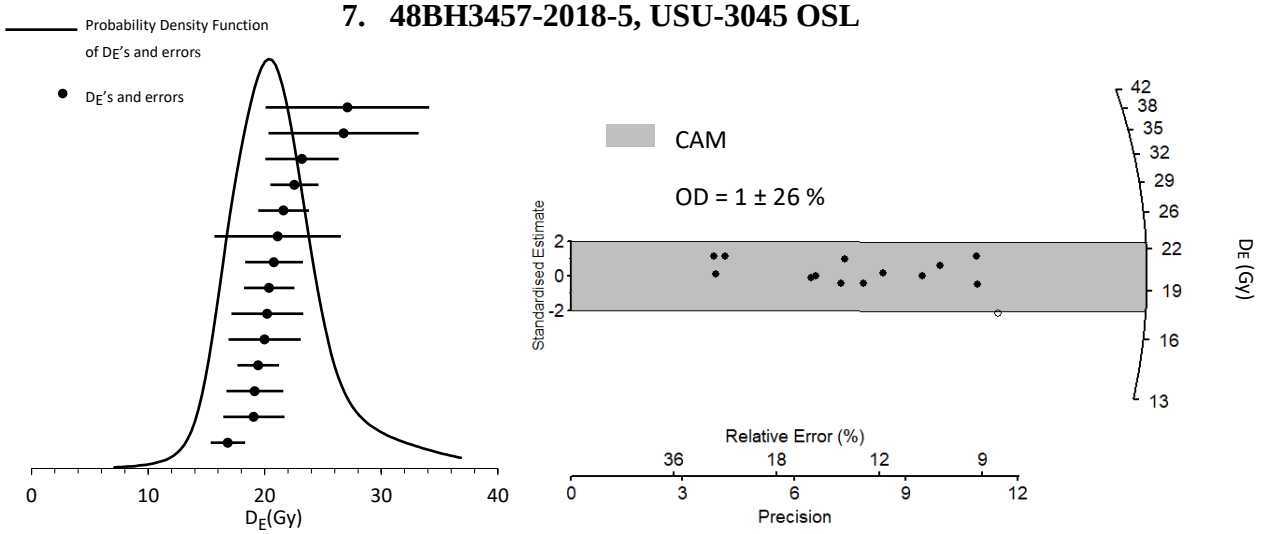

8. 48BH3457-2018-6, USU-3046 OSL

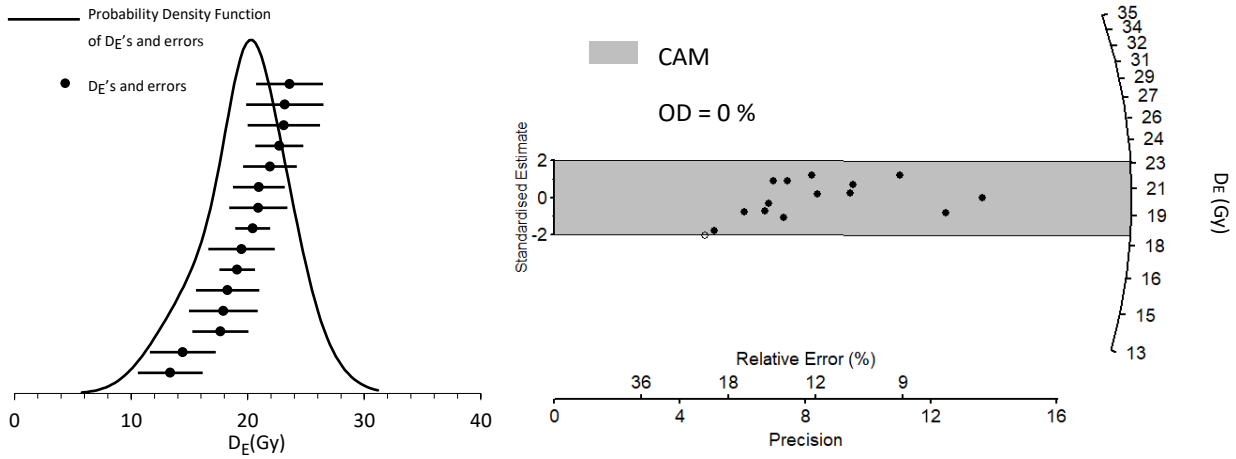

9. 48BH3457-2018-7, USU-3047 OSL

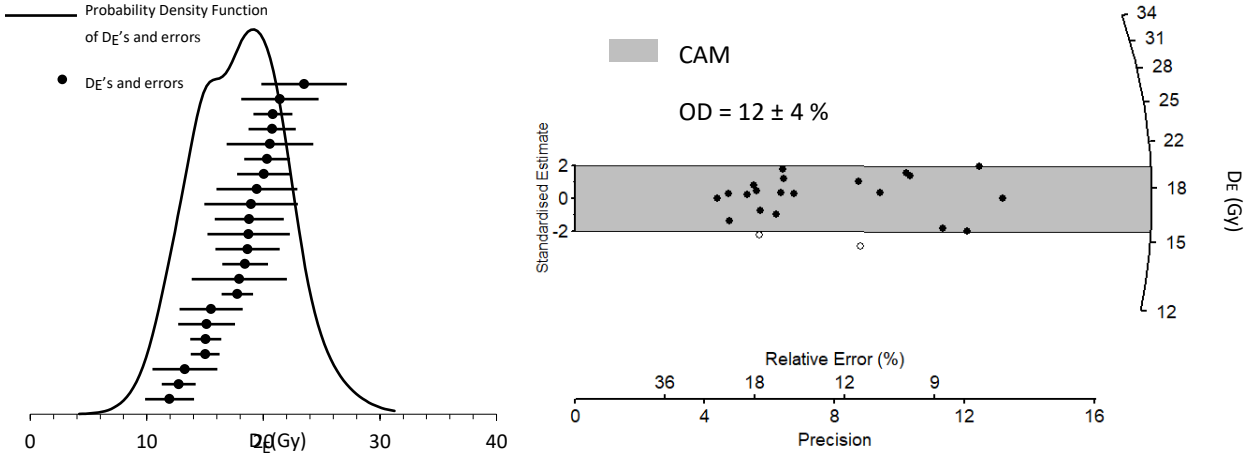

10. 48BH3457-2018-8, USU-3048

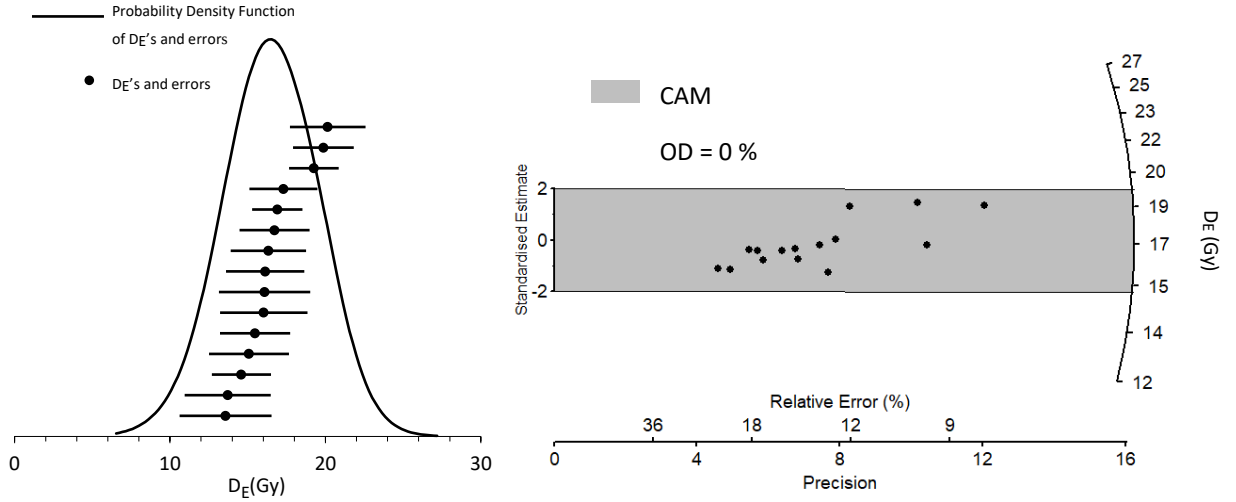

11. 48BH3457-2018-9, USU-3049 IRSL

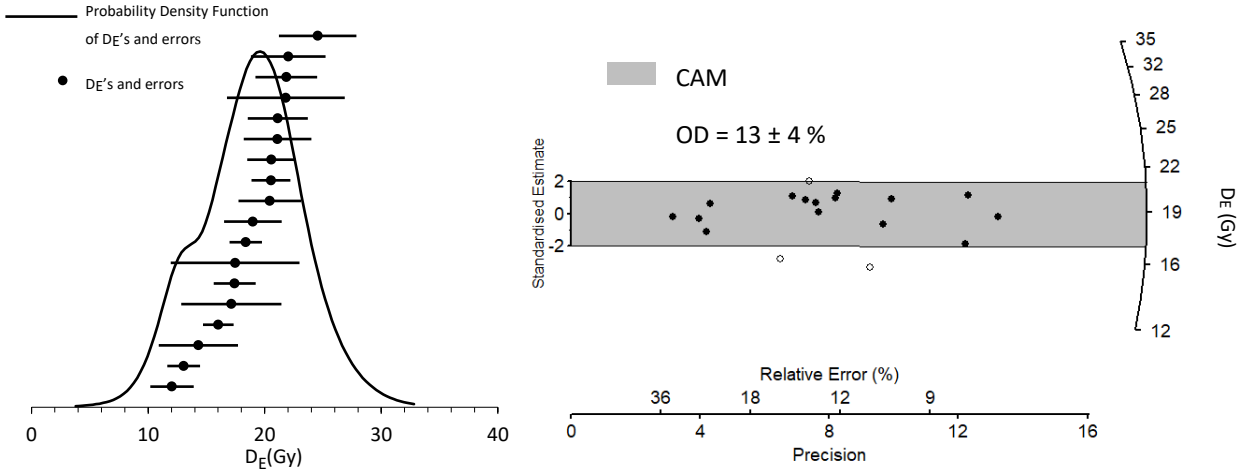

Appendix C: OxCal Age-Depth Model

Age-Depth Model with TP 1 Strata Code

```
Plot()
 {
  P_Sequence("Alm OSL",100,0,U(-2,2))
  {
   timescale="OSL";
   Boundary("Start Alm");
   Date("USU-3042",N(calBP(18320),2310))
   {
    z=3.45;
   };
   Date("USU-3041",N(calBP(14590),2110))
   {
    z=3.2;
   };
   Date("USU-3043",N(calBP(13950),1880))
   {
    z=2.75;
   };
   Boundary("Stratum 20/21")
   {
    z=2.45;
   };
   Date("USU-3044",N(calBP(13010),1400))
   {
    z=1.98;
   };
   Boundary("Stratum 18/19")
   {
    z=1.95;
   };
   Date("USU-3045",N(calBP(10400),1070))
   {
    z=1.9;
   };
   Date("USU-3046",N(calBP(10690),1060))
   {
    z=1.82;
   };
```

```
   Boundary("Stratum 17/18")
   {
    z=1.75;
   };
   Date("USU-3047",N(calBP(9250),1010))
   {
    z=1.68;
   };
   Boundary("Stratum 16/17")
   {
    z=1.60;
   };
   Date("USU-3048",N(calBP(9630),1000))
   {
    z=1.57;
   };
   Boundary("Stratum 14/15")
   {
    z=1.45;
   };
   Date("USU-3049",N(calBP(7230),860))
   {
    z=1.37;
   };
   Boundary("End Alm");
  };
 };
```

Age-Depth Model with Eolian Peaks Code

```
Plot()
 {
  P_Sequence("Alm OSL",100,0,U(-2,2))
  {
   timescale="OSL";
   Boundary("Start Alm");
   Date("USU-3042",N(calBP(18320),2310))
   {
    z=3.45;
   };
   Date("USU-3041",N(calBP(14590),2110))
   {
    z=3.2;
   };
   Date("USU-3043",N(calBP(13950),1880))
   {
    z=2.75;
   };
```

```
  Boundary("Eolian 4")
  {
   z=2.60;
  };
  Date("USU-3044",N(calBP(13010),1400))
  {
   z=1.98;
  };
  Date("USU-3045",N(calBP(10400),1070))
  {
   z=1.9;
  };
  Date("USU-3046",N(calBP(10690),1060))
  {
   z=1.82;
  };
  Boundary("Eolian 3")
  {
   z=1.75;
  };
  Date("USU-3047",N(calBP(9250),1010))
  {
   z=1.68;
  };
  Date("USU-3048",N(calBP(9630),1000))
  {
   z=1.57;
  };
  Boundary("Eolian 2")
  {
   z=1.55;
  };
  Date("USU-3049",N(calBP(7230),860))
  {
   z=1.37;
  };
  Boundary("Eolian 1")
  {
   z=1.32;
  };
  Boundary("End Alm");
 };
};
```

Figure 9. Alm Shelter with TP 1 strata boundaries (Figure 6a).

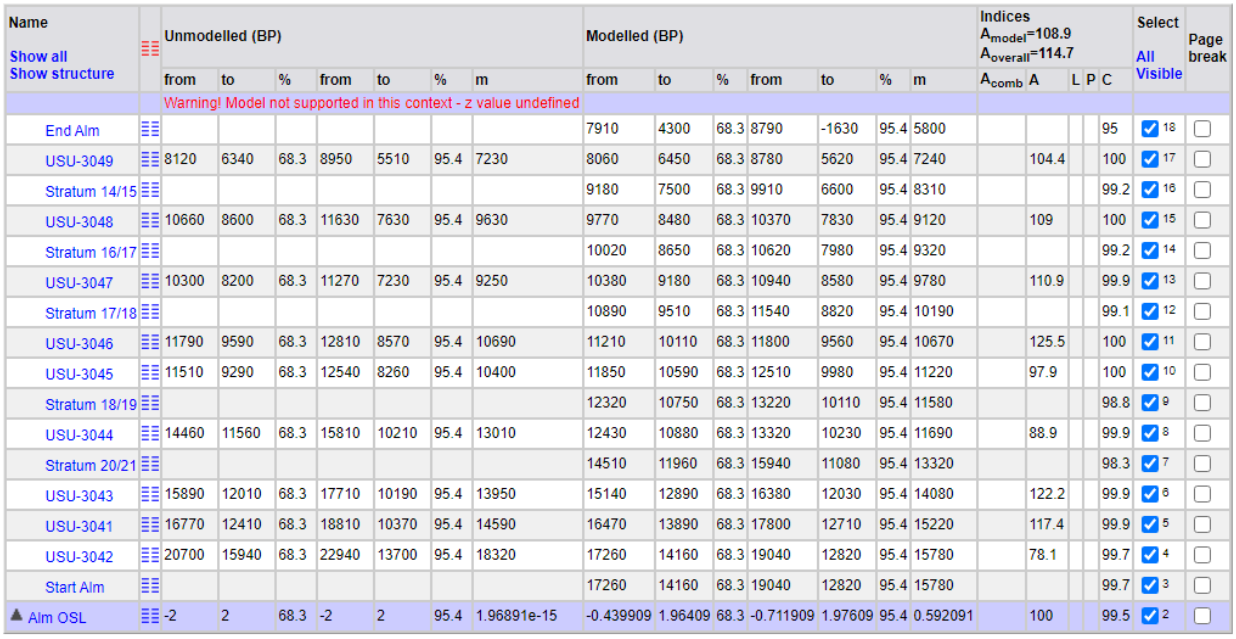

Name Show all Show structure		Unmodelled (BP)							Modelled (BP)							Indices A_{model}=108.9 $A_{overall}$=114.7					Select All Visible	Page break
		from	to	%	from	to	%	m	from	to	%	from	to	%	m	A_{comb}	A	L	P	C		
		Warning! Model not supported in this context - z value undefined																				
End Alm									7910	4300	68.3	8790	-1630	95.4	5800					95	18	
USU-3049		8120	6340	68.3	8950	5510	95.4	7230	8060	6450	68.3	8780	5620	95.4	7240		104.4			100	17	
Stratum 14/15									9180	7500	68.3	9910	6600	95.4	8310					99.2	16	
USU-3048		10660	8600	68.3	11630	7630	95.4	9630	9770	8480	68.3	10370	7830	95.4	9120		109			100	15	
Stratum 16/17									10020	8650	68.3	10620	7980	95.4	9320					99.2	14	
USU-3047		10300	8200	68.3	11270	7230	95.4	9250	10380	9180	68.3	10940	8580	95.4	9780		110.9			99.9	13	
Stratum 17/18									10890	9510	68.3	11540	8820	95.4	10190					99.1	12	
USU-3046		11790	9590	68.3	12810	8570	95.4	10690	11210	10110	68.3	11800	9560	95.4	10670		125.5			100	11	
USU-3045		11510	9290	68.3	12540	8260	95.4	10400	11850	10590	68.3	12510	9980	95.4	11220		97.9			100	10	
Stratum 18/19									12320	10750	68.3	13220	10110	95.4	11580					98.8	9	
USU-3044		14460	11560	68.3	15810	10210	95.4	13010	12430	10880	68.3	13320	10230	95.4	11690		88.9			99.9	8	
Stratum 20/21									14510	11960	68.3	15940	11080	95.4	13320					98.3	7	
USU-3043		15890	12010	68.3	17710	10190	95.4	13950	15140	12890	68.3	16380	12030	95.4	14080		122.2			99.9	6	
USU-3041		16770	12410	68.3	18810	10370	95.4	14590	16470	13890	68.3	17800	12710	95.4	15220		117.4			99.9	5	
USU-3042		20700	15940	68.3	22940	13700	95.4	18320	17260	14160	68.3	19040	12820	95.4	15780		78.1			99.7	4	
Start Alm									17260	14160	68.3	19040	12820	95.4	15780					99.7	3	
▲ Alm OSL		-2	2	68.3	-2	2	95.4	1.96891e-15	-0.439909	1.96409	68.3	-0.711909	1.97609	95.4	0.592091		100			99.5	2	

Figure 10. Alm Shelter with grain-size peaks output table (Figure 6b).

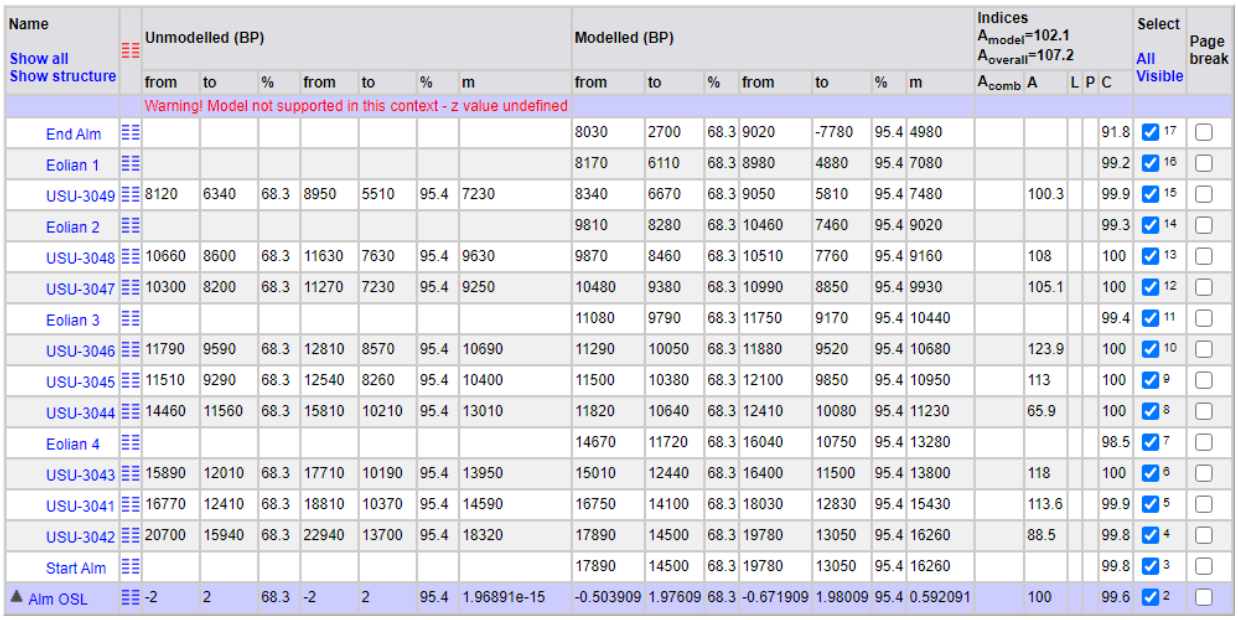

Name Show all Show structure		Unmodelled (BP)							Modelled (BP)							Indices A_{model}=102.1 $A_{overall}$=107.2					Select All Visible	Page break
		from	to	%	from	to	%	m	from	to	%	from	to	%	m	A_{comb}	A	L	P	C		
		Warning! Model not supported in this context - z value undefined																				
End Alm									8030	2700	68.3	9020	-7780	95.4	4980					91.8	17	
Eolian 1									8170	6110	68.3	8980	4880	95.4	7080					99.2	16	
USU-3049		8120	6340	68.3	8950	5510	95.4	7230	8340	6670	68.3	9050	5810	95.4	7480		100.3			99.9	15	
Eolian 2									9810	8280	68.3	10460	7460	95.4	9020					99.3	14	
USU-3048		10660	8600	68.3	11630	7630	95.4	9630	9870	8460	68.3	10510	7760	95.4	9160		108			100	13	
USU-3047		10300	8200	68.3	11270	7230	95.4	9250	10480	9380	68.3	10990	8850	95.4	9930		105.1			100	12	
Eolian 3									11080	9790	68.3	11750	9170	95.4	10440					99.4	11	
USU-3046		11790	9590	68.3	12810	8570	95.4	10690	11290	10050	68.3	11880	9520	95.4	10680		123.9			100	10	
USU-3045		11510	9290	68.3	12540	8260	95.4	10400	11500	10380	68.3	12100	9850	95.4	10950		113			100	9	
USU-3044		14460	11560	68.3	15810	10210	95.4	13010	11820	10640	68.3	12410	10080	95.4	11230		65.9			100	8	
Eolian 4									14670	11720	68.3	16040	10750	95.4	13280					98.5	7	
USU-3043		15890	12010	68.3	17710	10190	95.4	13950	15010	12440	68.3	16400	11500	95.4	13800		118			100	6	
USU-3041		16770	12410	68.3	18810	10370	95.4	14590	16750	14100	68.3	18030	12830	95.4	15430		113.6			99.9	5	
USU-3042		20700	15940	68.3	22940	13700	95.4	18320	17890	14500	68.3	19780	13050	95.4	16260		88.5			99.8	4	
Start Alm									17890	14500	68.3	19780	13050	95.4	16260					99.8	3	
▲ Alm OSL		-2	2	68.3	-2	2	95.4	1.96891e-15	-0.503909	1.97609	68.3	-0.671909	1.98009	95.4	0.592091		100			99.6	2	

Appendix D: Climate Proxies

Climate Comparison Scatterplot R Code

```
library(tidyverse)


proxy <- readr::read_csv("C:\\Users\\Cayla\\Documents\\Grad
School\\Thesis\\Alm Shelter\\Post-Defense Final
Drafts\\ClimateProxies_Data.csv")


#proxy graph ----

ggplot() +


#make the background boxes manually

  geom_rect(data=NULL,

            aes(xmin=12700,

                xmax=13200,

                ymin=-Inf,

                ymax=Inf),

            fill="gray80")+

  geom_rect(data=NULL,

            aes(xmin=8700,

                xmax=10700,

                ymin=-Inf,

                ymax=Inf),

            fill="gray80")+

  geom_rect(data=NULL,

            aes(xmin=6800,

                xmax=7400,
```

```
                ymin=-Inf,
                ymax=Inf),
            fill="gray80")+


#make the datapoints
  geom_point(
    data = ClimateProxies_Data %>%
      dplyr::filter( !is.na(`Location`)),
    aes(y = rowname,
        color = factor(Index.Type), # note that point colors
match error bar colors
        x = midDate, #middate point for visualization
        shape = factor(Index.Type)),
    size = 5) + #change point size
    scale_shape_manual(
      values = c(18, 18, 15, 16, 17)) + # unique point shapes
that are distinguishable
    scale_color_manual(values= c( "gray30", "black",
"darkorange", "dodgerblue4", "deeppink")
    ) +


#make the horizontal errorbars
  geom_errorbarh(
    data = ClimateProxies_Data %>%
      dplyr::filter( !is.na(`Location`)),
    aes(y = rowname,
        color = factor(Index.Type), #unique colors by location
        xmax = `Start.Date`,
        xmin = `End.Date`,
        height = 0.7), #error bar tail height
```

```
    size = 1 ) + #thickness of line


#create the site labels
  geom_rect(data=NULL, #Create Blue Lake label
            aes(xmin=5000,
                xmax=15000,
                ymin=26.5,
                ymax=27.5),
            fill= NA,
            color = "black")+
    annotate(geom = "label", x=14000, y=27, label="Blue Lake",
label.size = NA, size = 3.5)+
  geom_rect(data=NULL, #Create Stonehouse Meadow label
            aes(xmin=5000,
                xmax=15000,
                ymin=25.5,
                ymax=26.5),
            fill= NA,
            color = "black")+
   annotate(geom = "label", x=14000, y=26, label="Stonehouse
Meadow", label.size = NA, size = 3.5)+
  geom_rect(data=NULL, #Create St. Anthony Dune Label
            aes(xmin=5000,
                xmax=15000,
                ymin=24.5,
                ymax=25.5),
            fill= NA,
            color = "black")+
   annotate(geom = "label", x=14000, y=25, label="St. Anthony
Dunes", label.size = NA, size = 3.5)+
```

```
  geom_rect(data=NULL, #Create Lake of the Woods Label
            aes(xmin=5000,
                xmax=15000,
                ymin=21.5,
                ymax=24.5),
            fill= NA,
            color = "black")+
   annotate(geom = "label", x=14000, y=23, label="Lake of the
Woods", label.size = NA, size = 3.5)+
  geom_rect(data=NULL, #Create Killpecker Dunes Label
            aes(xmin=5000,
                xmax=15000,
                ymin=18.5,
                ymax=21.5),
            fill= NA,
            color = "black")+
   annotate(geom = "label", x=14000, y=20, label="Killpecker
Dunes", label.size = NA, size = 3.5)+
  geom_rect(data=NULL, #Create Buckbean Fen and Sherd Lake Label
            aes(xmin=5000,
                xmax=15000,
                ymin=17.5,
                ymax=18.5),
            fill= NA,
            color = "black")+
   annotate(geom = "label", x=14000, y=18, label="Buckbean Fen
and Sherd Lake", label.size = NA, size = 3.5)+
  geom_rect(data=NULL, #Create Ferris Dunes Label
            aes(xmin=5000,
                xmax=15000,
```

```
                ymin=16.5,
                ymax=17.5),
            fill= NA,
            color = "black")+
   annotate(geom = "label", x=14000, y=17, label="Ferris Dunes",
label.size = NA, size = 3.5)+
  geom_rect(data=NULL, #Create Casper Dunes Label
            aes(xmin=5000,
                xmax=15000,
                ymin=15.5,
                ymax=16.5),
            fill= NA,
            color = "black")+
   annotate(geom = "label", x=14000, y=16, label="Casper Dunes",
label.size = NA, size = 3.5)+
  geom_rect(data=NULL, #Create Kettle Lake Label
            aes(xmin=5000,
                xmax=15000,
                ymin=11.5,
                ymax=15.5),
            fill= NA,
            color = "black")+
   annotate(geom = "label", x=14000, y=13.5, label="Kettle
Lake", label.size = NA, size = 3.5)+
  geom_rect(data=NULL, #Create Nebraska Sand Hills Label
            aes(xmin=5000,
                xmax=15000,
                ymin=6.5,
                ymax=11.5),
            fill= NA,
```

```
            color = "black")+
   annotate(geom = "label", x=14000, y=9, label="Nebraska Sand
Hills", label.size = NA, size = 3.5)+
  geom_rect(data=NULL, #Create Alm Shelter Grain Size Label
            aes(xmin=5000,
                xmax=15000,
                ymin=2.5,
                ymax=6.5),
            fill= NA,
            color = "black")+
   annotate(geom = "label", x=14000, y=4.5, label="Alm Shelter
Grain Size", label.size = NA, size = 3.5)+
  geom_rect(data=NULL, #Create Alm Shelter Luminescence Label
            aes(xmin=5000,
                xmax=15000,
                ymin=-3.5,
                ymax=2.5),
            fill= NA,
            color = "black")+
   annotate(geom = "label", x=14000, y=-0.5, label="Alm Shelter
Luminescence", label.size = NA, size = 3.5)+

#vertical lines for the panel grid
  geom_vline(xintercept = seq(4500, 15500, 500),
             linetype = "dotted",
             color = "gray30") +

#flip for BP visibility
  scale_x_reverse(breaks = seq(4500, 15500, 500)) +
```

```
#label
  labs(x = "Year Before 1950") +


#title
  ggtitle("Regional Climate Records")+


#basic theme to minimize visual noise
  theme_minimal() +
  theme(
    plot.title = element_text (size = 25, hjust = 0.5), #title
    legend.position = "top",
    legend.text = element_text(size = 12),
    axis.title.y = element_blank(), #removes the y label
    axis.text.y = element_blank(), #remove y tick labels
    axis.title.x = element_text(size = 16),
    axis.text.x = element_text(angle = 90, vjust = 0.5, hjust=1,
size = 12),
    legend.title = element_blank(), #removes legend title
    panel.grid = element_blank() #removes the background grid
pattern
  )
```

Table 7. ClimateProxies_Data.

	Row name	Location	Source	DateType	BP Dates	Start Date	End Date	Index Type	midDate
31	27	Blue Lake	Louderback and Rhode 2009	cal yr BP	8300-6500	8300	6500	Moisture	7400
30	26	Stonehouse Meadow	Mensing et al. 2013	cal yr BP	7500-5000	7500	5000	Moisture	6250
29	25	St. Anthony Dunes	Rich et al. 2015	ka	6525	6525	6525	Dune	6525
28	24	Lake of the Woods	Shuman et al. 2010	ka	6140-4640	6140	4640	Moisture	5390
27	23	Lake of the Woods	Shuman et al. 2010	ka	9040-6140	9040	6140	Moisture	7590
26	22	Lake of the Woods	Shuman et al. 2010	ka	11240	11240	11240	Moisture	11240
25	21	Killpecker Dunes	Mayer and Mahan 2004	cal yr BP	8800-8100*	8800	8800	Dune	8800
24	20	Killpecker Dunes	Mayer and Mahan 2004	cal yr BP	11500-10200	11500	10200	Dune	10850
23	19	Killpecker Dunes	Ahlbrandt et al. 1983	RCYBP	11690-9910	11690	9910	Dune	10800
22	18	Buckbean Fen and Sherd Lake	Shuman 2012	cal yr BP	9000-6000	9000	6000	Temp	7500
21	17	Ferris Dunes	Stokes and Gaylord 1993	ka	8757-8057	8757	8057	Dune	8407
20	16	Casper Dunes	Halfen et al. 2010	ka	9940-6140	9940	6140	Dune	8040
19	15	Kettle Lake	Grimm et al. 2011	cal yr BP	6250	6250	6250	Moisture	6250
18	14	Kettle Lake	Grimm et al. 2011	cal yr BP	9250	9250	9250	Moisture	9250
17	13	Kettle Lake	Grimm et al. 2011	cal yr BP	10730	10730	10730	Moisture	10730
16	12	Kettle Lake	Grimm et al. 2011	cal yr BP	12750	12750	12750	Moisture	12750

15	11	Nebraska Sand Hills	Loope et al. 1995	RCYBP	7480-330	7480	5000	Dune	5000
14	10	Nebraska Sand Hills	Ahlbrandt et al. 1983	RCYBP	8540-7330	8540	7330	Dune	7935
13	9	Nebraska Sand Hills	Miao et al. 2007	ka	9543-6443	9543	6443	Dune	7993
12	8	Nebraska Sand Hills	Ahlbrandt et al. 1983	RCYBP	13070-11280	13070	11280	Dune	12175
11	7	Nebraska Sand Hills	Loope et al. 1995	RCYBP	13290-12750	13290	12750	Dune	13020
10	6	Alm Shelter Grain Size	na	cal yr BP	8950-4970	8950	4970	Alm Shelter Grain Size	6960
9	5	Alm Shelter Grain Size	na	cal yr BP	10280-7450	10280	7450	Alm Shelter Grain Size	8865
8	4	Alm Shelter Grain Size	na	cal yr BP	11460-8600	11460	8600	Alm Shelter Grain Size	10030
7	3	Alm Shelter Grain Size	na	cal yr BP	14180-10360	14180	10360	Alm Shelter Grain Size	12270
6	2	Alm Shelter Lumin.	na	NA	8020-6300	8020	6300	Alm Shelter Luminescence	7160
5	1	Alm Shelter Lumin.	na	NA	10190-8170	10190	8170	Alm Shelter Luminescence	9180
4	0	Alm Shelter Lumin.	na	NA	10560-8560	10560	8560	Alm Shelter Luminescence	9560
3	-1	Alm Shelter Lumin.	na	NA	11400-9260	11400	9260	Alm Shelter Luminescence	10330
2	-2	Alm Shelter Lumin.	na	NA	11680-9560	11680	9560	Alm Shelter Luminescence	10620
1	-3	Alm Shelter Lumin.	na	NA	14340-11540	14340	11540	Alm Shelter Luminescence	12940